Electromagnetic wave propagation in two-dimensional photonic crystals: A study of anomalous refractive effects

S. Foteinopoulou[1,*] and C. M. Soukoulis[1,2]
[1]*Ames Laboratory-USDOE and Department of Physics and Astronomy, Iowa State University, Ames, Iowa 50011, USA*
[2]*Research Center of Crete, Heraklion, Crete 71110, Greece*
(Received 7 November 2003; revised manuscript received 23 May 2005; published 24 October 2005)

We systematically study a collection of refractive phenomena that can possibly occur at the interface of a two-dimensional photonic crystal with the use of the wave vector diagram formalism. Cases with a single propagating beam (in the positive or negative direction) as well as cases with birefringence were observed. We examine carefully the conditions to obtain a single propagating beam inside the photonic crystal lattice. Our results indicate that the presence of multiple reflected beams in the medium of incidence is neither a prerequisite nor does it imply multiple refracted beams. We characterize our results with respect to the origin of the propagating beam and the nature of propagation (left-handed or not). We identified four distinct cases that lead to a negatively refracted beam. Under these findings, the definition of phase velocity in a periodic medium is reexamined and its physical interpretation discussed. To determine the "rightness" of propagation, we propose a wedge-type experiment. We discuss the intricate details for an appropriate wedge design for different types of cases in triangular and square structures. We extend our theoretical analysis and examine our conclusions as one moves from the limit of photonic crystals with high-index contrast between the constituent dielectrics to photonic crystals with low modulation of the refractive index. Finally, we examine the "rightness" of propagation in the one-dimensional multilayer medium and obtain conditions that are different from those of two-dimensional systems.

DOI: 10.1103/PhysRevB.72.165112 PACS number(s): 78.20.Ci, 41.20.Jb, 42.25.−p, 42.30.−d

I. INTRODUCTION

Photonic crystals (PCs) are dielectric structures with two- or three-dimensional periodicity. They are known as the semiconductor counterpart for light, since they exhibit the ability—when engineered appropriately—to mold and control the propagation of electromagnetic (EM) waves. Among their unusual properties lies their ability to exhibit a wide variety of anomalous refractive effects, which recently attracted a great deal of interest, both theoretically[1–5] and experimentally.[6,7] The observed refractive effects can be quite complicated, and in most cases, the direction of the propagating signal cannot be interpreted with the use of a simple Snell-like formula. In particular, Kosaka *et al.*[6] observed a large swing of angle for the refracted beam for a small angle of incidence. They called this effect the "superprism phenomenon."

Anomalous refractive phenomena are known in the field of optics and are commonly associated with anisotropy in the optical properties of the material (permittivity).[8] Two propagating solutions exist, having a different dispersion relation. One of them is extraordinary—i.e., nonspherical. As a result, in some cases two refracted beams are observed in these media, a phenomenon known as "birefringence."[8,9] Numerous studies[10–14] on diffraction gratings, essentially the one-dimensional (1D) counterpart for the PC structures, led to the observation of a vast variety of anomalous refracted effects, including "birefringence." These systems have undergone extensive and systematic study[10–14] based on the wave vector diagram formalism. This formalism was proven to be an excellent tool in explaining the unusual refractive properties for the 1D diffraction grating system. The reader can find a didactic description of these diagrams and their use in Refs. 10 and 11.

Despite the recent interest focused on the superrefractive effects in two-dimensional crystals, a systematic study is certainly lacking in the literature for these systems and only a few effects were studied and discussed.[1–3,5,6,15] However, as we will demonstrate in this paper, a class of unusual propagation phenomena in PCs has yet not been demonstrated. Moreover, we will show that, contrary to one's intuition, the multiplicity of reflected beams in the incoming medium does not necessarily imply the presence of multiple beams in the PC medium and vice versa. In this context, we also investigate carefully the conditions necessary to obtain single-beam propagation inside a 2D square or triangular PC lattice.

The anomalous refractive effects observed in both the 1D grating and PC literature include cases where the light bends "the wrong way"—i.e., is refracted negatively at the air-PC interface. Such a phenomenon was observed and widely discussed in the left-handed materials literature.[16–19] In the left-handed medium (LHM), homogeneous[16] or composite,[17] the electric field vector **E**, the magnetic field vector **H**, and the wave vector **k** form a left-handed set of vectors. The sign of the product $\mathbf{S}\cdot\mathbf{k}$—**S** being the Poynting vector—reflects the sign of the "rightness" for the system[16] and is negative for the LHM. It is also customary to refer to a left-handed propagating wave as a backwards wave.[20] The refractive index for such a medium was calculated with the use of the scattering data and was found to be unambiguously negative.[19] However, the characterization of the left-handed or right-handed nature of propagation is a point somewhat overlooked in

both the 1D gratings and PC literature. Only in Ref. 5 was the sign of the product $\mathbf{S}\cdot\mathbf{k}$,[21] with $\mathbf{k}$ in the first Brillouin zone (BZ), determined for a two-dimensional triangular PC with a finite-difference time-domain simulation (FDTD).[22] The simulation experiment, performed on a wedged PC structure, is in accordance with the UCSD experiment.[23,24] In the latter, the negative index was experimentally verified for the traditional composite LHM. Left-handed behavior in photonic crystals relates to the origin and nature of a certain propagating beam. We intend to study this for different cases with the wave vector diagram formalism. In any case, the assignment of a proper refractive index should carry the information regarding the rightness of the PC medium in its sign and be consistent with the left-handed literature.

Moreover, the phase velocity for an EM wave propagating in a periodic structure is a subject of some controversy in the literature. Yariv defined the phase velocity for a propagating EM wave in the 1D layered medium as the phase velocity that corresponds to the dominant plane wave component.[25] Recently the phase velocity has been associated with the Bloch's crystal momentum $\mathbf{k}$, where $\mathbf{k}$ is in the first BZ.[1,5,26] Specifically, in Ref. 1 the phase velocity and appropriate phase index were discussed for both limits of index contrast between constituent dielectrics (high and low). Considering this controversy, the subject of phase velocity in a periodic medium should be reexamined. It is certainly worthwhile to reexamine the physical meaning of each definition in both limits of refractive index modulation (high and low).

In an attempt to make the study of the PC system simpler, in some cases the PC system was homogenized appropriately with the use of an effective medium theory.[27] However, these theories mainly apply to the long-wavelength limit. Nonetheless, as we will show in our subsequent analysis, for some cases that lie in the higher bands, it is still possible to characterize the refractive and propagation properties with an effective index $n(\omega)$ under certain conditions. It is important to examine carefully such conditions, since the study of the PC can be greatly simplified. We will see that in these cases, both phase and energy velocities can be derived by simple formulas.

In this work, we attempt a systematic study for the anomalous refractive phenomena occurring at the interface of two-dimensional PC systems. We focus on various cases that have substantially different origin. The characteristics of each case are analyzed. For this purpose, we discuss the phase and energy velocity of a propagating wave, as well as the corresponding "rightness." In particular, in Sec. II we present four distinct cases of anomalous refractive effects, where a negatively refracted beam is present. We explain and analyze the origin of the refracted beam with the wave vector diagrams in Sec. III. Using the same formalism, we also discuss the observed birefringent phenomena. We study all relevant properties which characterize an EM wave propagating inside the PC. In particular, we define appropriately a phase velocity, calculate it numerically, and discuss the meaning of the associated effective phase index in Secs. IV, V, and VI, respectively. Moreover, in Sec. VI we discuss the conditions necessary to obtain a single-beam propagation, which obeys a Snell-like formula, for 2D square and triangular PCs. Appropriate expressions for the group (energy) velocities are given in Sec. VII. In Sec. VIII, we discuss the group refractive index associated with the group velocity. In Sec. IX we focus our discussion on the left-or right-handed nature of propagation. In this section, we review the appropriate wedge experiment designs, which can unveil the sign of the "rightness" for different triangular and square PCs. In Sec. X, we discuss the validity of our theoretical analysis as one moves from the limit of high-index modulated crystals to the limit of photonic crystals with low-index modulation. Finally, we make a comparison between the two-dimensional PC medium and the 1D layered medium in Sec. XI. We present our conclusions in Sec. XII.

II. ANOMALOUS REFRACTIVE PHENOMENA AT THE AIR-PC INTERFACE

We present in Fig. 1 four characteristic cases where a negatively refracted beam appears when light is incident at a PC slab interface. The cases shown in Fig. 1 basically outline the different possible reasons for which a negatively refracted beam can appear inside the photonic crystal. In the case of Fig. 1(b), two distinct beams propagating in opposite directions (positive and negative) are present (birefringence). To study the various superrefractive effects, we employed the FDTD technique[22,28] with perfect matched layer[29] (PML) boundary conditions. We study various triangular PC structures of dielectric cylindrical pillars in air for the H (TE) polarization case (magnetic field aligned along the cylinder's axis). Whenever possible, we used the value of 12.96 for the dielectric constant and $r=0.35$ for the radius of the rods for consistency and comparison with the results in Ref. 5 and the results of Notomi.[1] However, sometimes for the purpose of isolating and observing clearly specific effects, it becomes necessary to employ PC structures with different parameters. The presence of a negatively refracted beam is clear in all four cases as seen in Figs. 1(a)–1(d). Before we expand our analysis, we discuss the wave vector diagrams. Careful use of such diagrams in the PC system can always explain and determine the direction(s) of the refracted beam(s). Then, we will be able to comment on the nature and origin of each different superrefractive effect shown in Fig. 1.

III. WAVE VECTOR DIAGRAMS AND INTERPRETATION OF THE FDTD RESULTS

Before we carry on with our analysis, we would like to discuss the phase matching condition[30] at the interface of a periodic structure. In the case of a homogeneous medium, this condition is represented in the conservation of the parallel to the interface component of the wave vector $k_{\parallel}$. In the case where the periodic medium is a diffraction grating, this condition has been generalized to

$$k_{\parallel,m} = \frac{\omega}{c}\sin\theta_{inc} + \frac{2\pi m}{b_{per}}, \tag{1}$$

where we consider EM waves incident from air with an angle θ_{inc} measured from the surface normal. m is an integer equal to $0, \pm 1, \pm 2$, and b_{per} represents the period of the 1D layered medium.[31] Note that $2\pi m/b_{per}$ is a reciprocal lattice vector

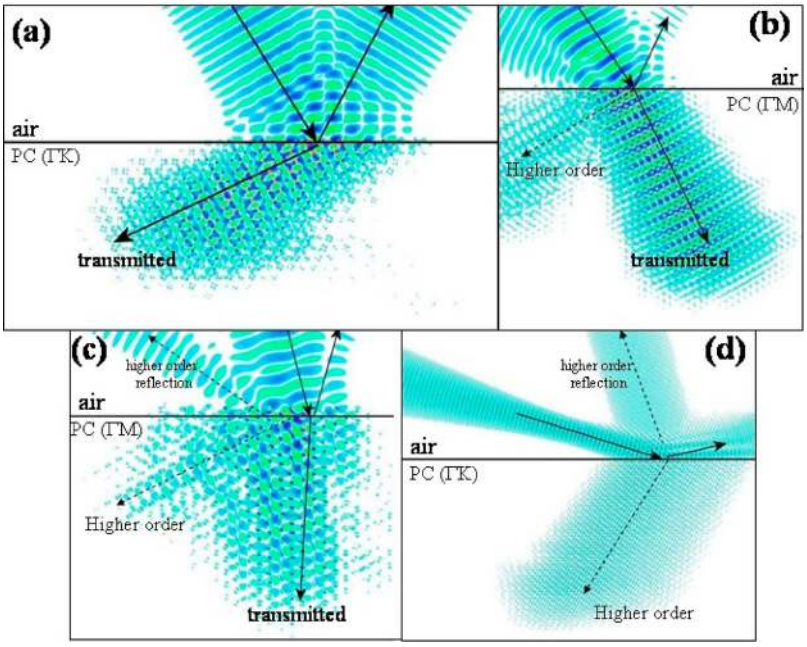

FIG. 1. (Color online) Oblique incidence of EM waves at photonic crystal slabs. The PC system consists of dielectric rods in a triangular arrangement. All cases are with magnetic field along the cylinders (H polarization). The parameters for each case (dielectric constant of rods, ϵ; radius of rods, r; and dimensionless frequency $\tilde{f}$) are (a) $\epsilon=12.96$, $r=0.35a$, $\tilde{f}=0.58$, (b) $\epsilon=20.0$, $r=0.37a$, $\tilde{f}=0.425$, (c) $\epsilon=12.96$, $r=0.35a$, $\tilde{f}=0.535$, and finally in (d) $\epsilon=7.0$, $r=0.35a$, $\tilde{f}=0.81$. Note that $\tilde{f}=fa/c=a/\lambda$, with a the lattice constant, c the velocity of light, and λ the wavelength of light in vacuum. The solid arrows indicate the transmitted, while the dotted black arrows indicate higher-order beams inside the PC.

of the 1D periodic system. Equation (1) has been used widely in the study of 1D diffraction gratings. We will refer to the phase matching condition of 1D systems, given by Eq. (1), as the Bragg formula in its known form. As a matter of fact, Eq. (1) also applies to 1D gratings with a slanted interface, with an angle ϕ in respect to the periodic direction, if a $\cos\phi$ factor is introduced on $2\pi m/b_{per}$.[32]

The same type of phase matching condition as given in Eq. (1) is also frequently used in 2D PC research.[33] In these cases, parameter b_{per} represents the distance between adjacent scatterers in real space (i.e., the period) along the interface, which is usually chosen along a symmetry direction of the 2D PC. For different interface cuts and lattice arrangements b_{per} is

$$b_{per}=\begin{cases} a & \text{for triangular cut along } \Gamma K, \\ \sqrt{3}a & \text{for triangular cut along } \Gamma M, \\ \sqrt{2}a & \text{for square cut along } \Gamma M, \\ a & \text{for square cut along } \Gamma X, \end{cases} \tag{R1}$$

with a being the lattice constant.

Nevertheless, caution must be exercised both in the interpretation and applicability of such a phase matching condition. For many 2D PCs, the quantity $2\pi/b_{per}$ ceases to represent a reciprocal lattice vector. In fact, in order to obtain an appropriate phase matching condition for 2D PCs, the lattice arrangement in the entire two-dimensional wave vector space must be considered. As we will see in more detail in Sec. IV, a propagating wave inside the photonic crystal has the form of a Floquet-Bloch (FB) wave, which consists of many plane waves. The FB wave is periodic in respect to the reciprocal lattice vector of the bulk 2D crystal (see the Appendix, part 2). Therefore, the projections of *all* reciprocal lattice vectors onto a certain interface (I) must be taken into account. It is not hard to check that for a triangular lattice these projections have periodicity $2\pi/b_{per}$, with $b_{per}=a$ and $\sqrt{3}a$ for an interface along ΓK, and ΓM, respectively. Therefore, we can still apply the Bragg formula as expressed in Eq. (1). Note, however, that the smallest reciprocal lattice vector along ΓK (ΓM) is $4\pi/a$ ($4\pi/\sqrt{3}a$). This value is twice the quantity in the familiar Bragg formula.

Still, a phase matching condition given by Eq. (1) should not be taken for granted for any general 2D system. In particular, cases involving slanted interfaces are intricate and require careful consideration.[34] Recently, other two-dimensional arrangements have been considered, such as rectangular PCs [35] or 2D PC lattices with a basis.[36] More complex cases, such as 2D PCs or 3D PCs with a basis also require careful consideration.[37,38] Actually, two lattices with common interface characteristics may be subject to a different phase matching condition.[37] Accordingly, the Bragg formula as expressed in Eq. (1) and its planar counterpart for a two- or three-dimensional periodic structure are not general. We stress that even when it does apply, it originates from the distribution of the modes in the entire 2D or 3D reciprocal space, respectively. In other words, the refractive behavior of 2D (3D) PCs can be very different from 1D (2D) diffraction gratings.

We intend to explain the anomalous refractive effects observed in Fig. 1 in an insightful manner and without any loss of generality. We do so by an appropriate adaptation of the wave vector diagram method, known from studies of one-dimensional periodic structures.[10–14] Such a framework can then also be applied in the study of any complex case. Note that in all the following, incident, reflected, or refracted angles will be always measured from the normal to the interface.

We make a small digression and discuss briefly how can one determine the directions of the reflected beams. As we mentioned earlier in this section the relevant quantity for the phase matching is the set of projections of *all* reciprocal

lattice vectors onto the interface. Consider a specific lattice type with an interface I and an incident beam with frequency ω coming from air with an angle θ_{inc}. We record the projections of all reciprocal lattice vectors $\mathbf{G}$'s onto the interface I, $G_{n,proj}$.[39] A reflected beam arises with an angle

$$\theta_{ref,n} = \sin^{-1} \frac{\omega/c \sin \theta_{inc} + G_{n,proj}}{\omega/c}, \tag{2}$$

when $|\omega/c \sin \theta_{inc} + G_{n,proj}| < \omega/c$. In many cases [see, for example, the cases in Eq. (R1)], these projections $G_{n,proj}$ are equal to $2n\pi/b_{per}$ with b_{per} the period along the interface. Thus, expression (2) becomes

$$\theta_{ref,n} = \sin^{-1} \frac{\omega/c \sin \theta_{inc} + 2n\pi/b_{per}}{\omega/c}, \tag{3}$$

with the condition $|\omega/c \sin \theta_{inc} + 2n\pi/b_{per}| < \omega/c$.

Let us proceed now with the determination of the refracted beams with the wave vector diagram formalism. The most important part of the wave vector diagram is the equifrequency surfaces (EFSs) that apply for the frequency of operation. Actually, for our two-dimensional system the surfaces reduce to contours. These contours consist of all allowed propagation modes in wave vector space that exist in the PC system for a certain frequency. One or a multiple set of contours can be relevant for a certain frequency, depending on the number of bands corresponding to the frequency of interest. To isolate the different superrefractive effects, we focus our study on cases with only one band corresponding to the frequency of interest. Basically, the wave vector diagram method consists of the following steps. First, we draw the EFS in the repeated zone scheme. Subsequently, we draw a line perpendicular to the interface representing the conservation of $k_{\|} = \omega/c \sin \theta_{inc}$. For consistency with existing nomenclature in the literature we refer to this line as the construction line from now on. Then, we take down *all* intersections between the construction line and the EFS. Afterward, we fold the intersections which fall outside the first BZ, back to the first BZ, by adding an appropriate reciprocal lattice vector. In the subsequent step, we record all the resulting wave vector values in the first BZ. These include the original intersections in the first BZ and those that were folded back from the higher zones. The reasoning behind this folding process relates to the nature of the FB wave.[40] In the Appendix, part 2, we show that the expressions of two FB waves that correspond to two wave vectors $\mathbf{k}_2$ and $\mathbf{k}_1$ are essentially equivalent if $\mathbf{k}_2 - \mathbf{k}_1 = \mathbf{G}$, with $\mathbf{G}$ being a reciprocal lattice vector. So for consistency we always express the FB wave in terms of a wave vector $\mathbf{k}$ lying in the first BZ. We refer to this wave vector as the fundamental wave vector[41] from now on. So, in other words, we perform the folding process in order to obtain the fundamental wave vector of the FB wave which corresponds to a certain wave vector intersection.

Now, a last step remains. This is to determine the actual propagation direction of the signal that corresponds to each value of the set of fundamental wave vectors, which was determined from the above procedure. Evidently, different wave vector intersections that correspond to the same fundamental wave vector yield one and only one refracted beam. We refer to these intersections as "equivalent." Only different wave vector points that result in the first zone after the folding process can give rise to different beams. To carry on with our wave vector diagram analysis we need one more information. This is the sign of the slope $(\mathbf{k} \cdot \nabla \omega)$ of the band for the frequency we study. The refracted beam (signal) travels along the direction of its energy velocity. We discuss in Sec. VII that the energy velocity $\mathbf{v}_e$ is equal to the group velocity $\mathbf{v}_g$ for the photonic crystal. Now, $\mathbf{v}_g$ is $\nabla_{\mathbf{k}}\omega$. Moreover, the geometric properties of the gradient imply that group velocity $\mathbf{v}_g$ is normal to the EFS at a certain wave vector point in $\mathbf{k}$ space and points towards increasing frequencies ω. An additional restriction applies concerning the causality of the signal. From all the different directions for the refracted signal(s) we determine, only those pointing away from the source can be accepted. We stress that in the wave vector diagram analysis one construction line suffices when all modes are taken into account in the repeated zone scheme. This is because the phase matching condition itself stems from the repetition of the modes in the reciprocal space. Thus, it is redundant to draw multiple construction lines depicting the Bragg formula as given by Eq. (1). In fact, in some cases, such as PCs with a slanted interface, it becomes entirely inappropriate, and only the construction line should be drawn in such cases.[34] Summarizing, in a general 2D PC case, we have fixed frequency (represented by the EFS contour), fixed band slope (sign of $\nabla_{\mathbf{k}}\omega \cdot \mathbf{k}$), and fixed parallel component of wave vector (represented by the construction line). This is all the information we need to determine all refracted beams. We follow exactly the same steps of the approach which we described above for all the cases shown in Fig. 1. We categorize the refracted beams according to their order. A beam corresponding to an intersection lying in the first BZ, which did not need folding, is a zeroth-order beam. We call this beam "transmitted" beam in the following. On the other hand, beams stemming from intersections in the higher zones, which were subsequently folded back to the first zone, are classified as higher-order beams.

In Fig. 2 we show the wave vector diagram for the case of Fig. 1(a) drawn in the repeated zone scheme. Note that all the EFSs are calculated with the use of the plane wave expansion (PWE) method. We note that whenever we refer to the PWE method[42–44] for the H-polarization case, we applied Ho's method instead of the inverse expansion method, since the former is proven to show faster convergence.[43–45] The bold green dot-dashed line in Fig. 2 represents the construction line. It intersects points A and B of the EFS in the first zone (black circle) and points $A2$, $B2$, $A3$, and $B3$ of the EFSs in the higher-order zones. We fold points $A2$, $B2$, $A3$, and $B3$ back to the first zone by adding $\mathbf{G}_n = n\,\mathbf{G}_{0y}$ (see figure) (where $n=-2$ for points $A2$ and $B2$ and $n=+2$ for $A3$ and $B3$). Notice they all fall back onto points A and B. The case of Fig. 2 corresponds to a band with negative slope. Therefore, A has $\mathbf{v}_e$ pointing away from the source, while B has $\mathbf{v}_e$ pointing towards the source. This means that only point A contributes to a propagating beam, which is a "transmitted" beam. We indicate the propagating beam with the bold orange arrow in Fig. 2 and the bold solid arrow in the

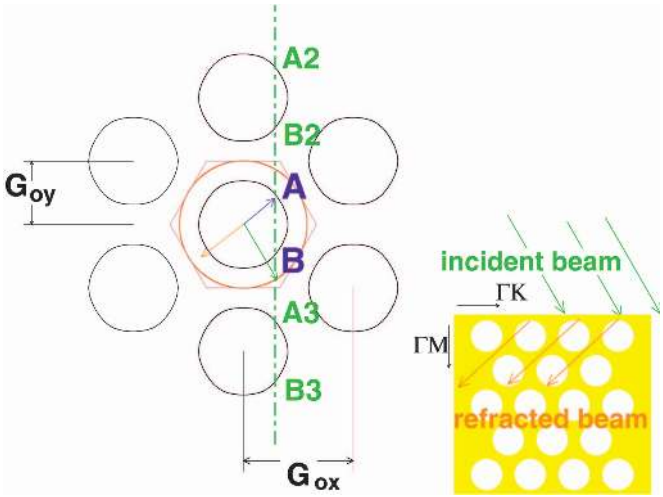

FIG. 2. (Color) Wave vector diagram for the case of Fig. 1(a). The equifrequency surfaces are plotted (black solid lines) in the repeated zone scheme. The red solid circle represents the equifrequency surface for the air (incoming) medium. The green dot-dashed line is the construction line. All intersections between construction line and EFSs are indicated ($A,B,A2,B2,A3,B3$). The intersections in the higher-order zones, $A2,B2,A3,B3$, fall onto A and B, respectively, when folded back to the first BZ. The blue vector represents the fundamental wave vector of the FB wave that corresponds to a causal signal. The respective energy velocity that coincides with the propagating signals direction is shown as the orange vector. For this cut $G_{0x,y}=2\pi/a_{x,y}$ with $a_x=a$ (lattice constant) and $a_y=\sqrt{3}a$. A general reciprocal lattice vector is $(2n1+n2)\ \mathbf{G}_{0x}+n2\ \mathbf{G}_{0y}$, with $n1,n2$ integers.

FDTD simulation in Fig. 1(a). We note that the negative refraction we observe in this case is similar in nature to the one occurring in a homogeneous medium with a negative refractive index.[16,46] We see that the perpendicular component of the wave vector has reversed sign at the interface. Also, the "transmitted" beam in this case has the fundamental wave vector and energy velocity "almost" antiparallel.

In Fig. 1(b) we see that two beams coexist (birefringence). This case corresponds to a band with positive slope ($\mathbf{v}_e\cdot\mathbf{k}>0$). The corresponding wave vector diagram in the repeated zone scheme is shown in Fig. 3. The green bold dot-dashed line in the diagram is the construction line for this case representing $k_{\|}=\omega/c\ \sin\theta_{inc}$. We find that this line intersects points A and B in the first BZ, as well as points $A2$, $B2$ and $A3$, $B3$ in the other zones. We need to fold points $A2$, $B2$, $A3$, and $B3$ back in the first BZ in order to acquire the value of the fundamental wave vector of the corresponding FB wave. We perform this folding by adding $\mathbf{G}=-\mathbf{G}_{0x}+n\mathbf{G}_{0y}$ with $n=-1$ for points $A2$ and $B2$ and $n=+1$ for points $A3$ and $B3$. We observe that the points $A2$, $A3$ ($B2,B3$) fall after the folding process onto point A' (B'). Note that each different wave vector point within the first zone after the folding process corresponds to a different FB wave and therefore to a different beam. However, from the entire set of wave vector points resulting in the first zone—i.e., A, B, A', B'—only B and B' correspond to a signal that propagates away from the source and therefore give rise to a propagating beam. We have therefore two propagating beams, one stemming from point B and one from point B'. Their respective signals are indicated with the bold and dotted orange vector in Fig. 3. They correspond to the bold and dotted black arrows in the FDTD simulation of Fig. 1(b). Actually, the first beam [solid arrow in Fig. 1(b)] is the "transmitted" beam, since B is a direct intersection of the construction line and the first BZ. Nevertheless, the beam that corresponds to the dotted arrow clearly stems from an intersection originally lying in a higher-order zone—i.e., is a higher-order effect.

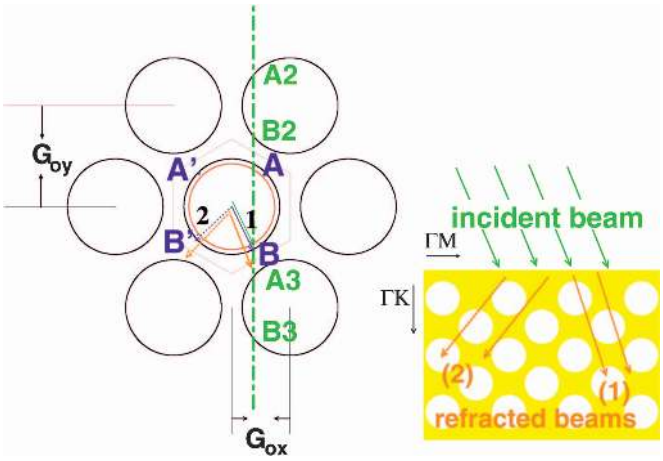

FIG. 3. (Color) Wave vector diagram for the case of Fig. 1(b). The equifrequency surfaces are plotted (black solid lines) in the repeated zone scheme. The red solid circle represents the equifrequency surface for the air (incoming) medium. The green dot-dashed line is the construction line. All intersections are indicated. The blue vectors represent the intersections that result in the first zone after the folding process and correspond to causal signal (shown as the orange vectors). For this cut $G_{0x,y}=2\pi/a_{x,y}$ with $a_x=\sqrt{3}a$ (lattice constant) and $a_y=a$. A general reciprocal lattice vector is $n1\ \mathbf{G}_{0x}+(n1+2n2)\ \mathbf{G}_{0y}$, with $n1,n2$ integers.

In Fig. 4 we see the EFS plotted in the repeated zone scheme for the case of Fig. 1(c). The construction line (green bold dot-dashed line) intersects points A and B in the first Brillouin zone and points $A2$, $B2$, $A3$, and $B3$ in the higher-order zones. The latter fall onto points A' and B' when they are folded back to the first zone (with a similar process as in Fig. 3). Thus, following the folding process, the set of wave vector intersections inside the first zone consists of points A,

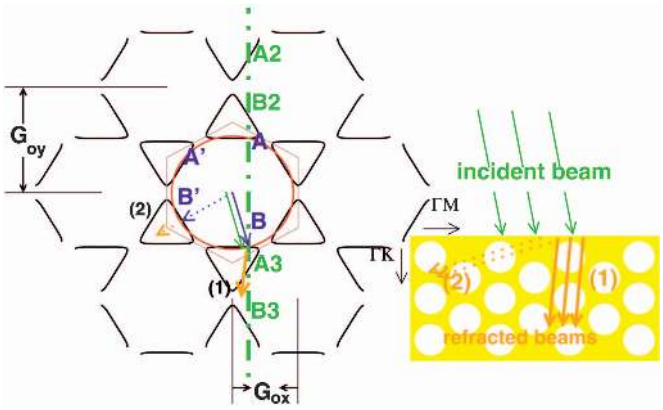

FIG. 4. (Color) Same as Fig. 4 but for the case of Fig. 1(c).

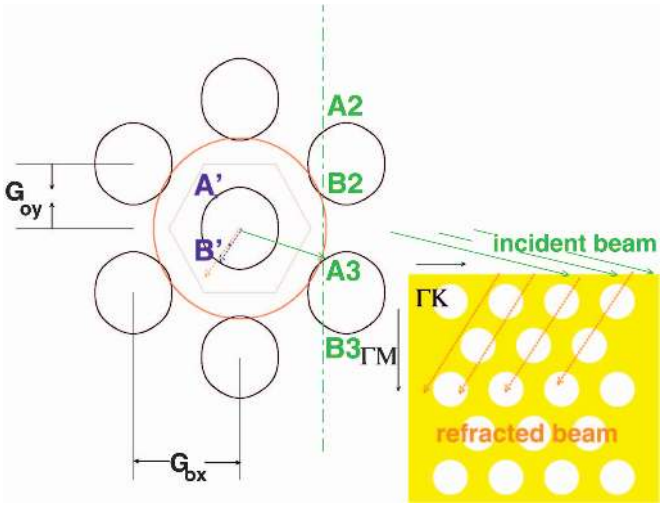

FIG. 5. (Color) Wave vector diagram for the case of Fig. 1(d) in the extended zone scheme. For this cut $G_{0x,y}=2\pi/a_{x,y}$ with $a_x=a$ (lattice constant) and $a_y=\sqrt{3}a$. A general reciprocal lattice vector is $(2n1+n2)\ \mathbf{G}_{0x}+n2\ \mathbf{G}_{0y}$, with $n1,n2$ integers. Everything else is the same as in the previous figures.

B, A', and B'. Taking into account the sign of $\mathbf{v}_e\cdot\mathbf{k}$, in this case positive, from all these intersections, only B and B' yield a causal propagating beam that we indicate with a bold and dotted orange arrow in Fig. 4, respectively. For the same exact reason, as in the case of Fig. 3, the bold arrow representing the beam corresponding to point B is the "transmitted" beam. The dotted arrow, which represents the beam corresponding to point B', is a higher-order beam. Note that in this case both transmitted and higher-order beams are in the negative direction. This is caused by the particular shape of the EFS for this case—i.e., anisotropic and broken with sixfold symmetry. This is the basic difference between the cases of Figs. 3 and 4. In every other respect, the origin of the higher-order beam, and thus observation of the birefringent effect, in the cases of Figs. 3 and 4 is identical.

In Fig. 5 we show the wave vector diagrams in the repeated zone scheme that corresponds to the case of Fig. 1(d). The $\mathbf{k}_\parallel$ conservation line intersects no points in the first BZ and several points $(A2,B2,A3,B3)$ in the higher-order zones. However, all of these points when folded back in the first BZ fall onto either point A' or B'. In other words, they are equivalent to points A' and B', respectively. Since $\mathbf{v}_e\cdot\mathbf{k}>0$, only the wave vector at B' corresponds to a causal propagating FB wave, with energy velocity indicated by an orange dotted arrow in the figure. This is the sole propagating beam shown with a black dotted arrow in the corresponding FDTD simulation in Fig. 1(d). Essentially, in this case we have only a higher-order beam and no "transmitted" beam.

Notice the excellent agreement between the theoretical prediction—derived from the wave vector diagrams—and the actual FDTD simulations seen in Fig. 1. In all cases the interface lies along a symmetry direction. However, we stress that our preceding analysis is general and succeeds in the determination of the propagating beams for even complex 2D PCs, such as those involving a slanted interface, which does not lie along a symmetry direction.[34] We tested our predictions for a specific case of this type and indeed found very good agreement with the corresponding FDTD results.[34] For the reader's benefit, we mention at this point that for any general case, when the appropriate phase matching condition is derived one can follow an alternative approach. This involves drawing the EFS in the first Brillouin zone and keeping multiple construction lines representing the applicable phase matching condition. As we mentioned before, this condition must be derived on a case by case basis and may be different from expression (1). Both approaches are in fact entirely equivalent. A graphical approach though in the repeated zone scheme may provide more insight into the origin of the refracted beams. For example, as we will explain in the following the presence of the second beam in Fig. 1(b) is associated with the two-dimensional periodic nature of the crystal. We believe that the wave vector methodology in the repeated zone scheme can be easily generalized for 3D PCs and uncover many interesting superrefractive effects in such systems.

Before we conclude this section we would like to discuss further a few interesting observations regarding our results in Figs. 2–5. One point concerns the "transmitted" beams (solid orange arrows in Fig. 2–4) and the higher-order beams (dotted orange arrows in Figs. 3–5). Notice from the figures that all "transmitted" beams have fundamental wave vector $\mathbf{k}_t$ (bold blue arrows in Figs. 2–4) with projection onto the interface equal to $k_\parallel$ of the incident beam. However, the higher-order beams have fundamental wave vector $\mathbf{k}_{ho}$ (dotted blue arrows in Figs. 3–5) with projection onto the interface different from $k_\parallel$ of the incident beam. In fact $k_{ho,\parallel}=k_\parallel-2\pi/b_{per}$. In this context we can say that the "transmitted" beams are *direct* refracted beams while the higher-order beams are *umklapp* refracted beams. The different anomalous refracted effects reported so far in 2D PC literature[1–5] involve direct processes only. So one can observe the formation of a negatively refracted beam through a direct process [bold arrows in Figs. 1(a) and 1(c)] or through an umklapp process [dotted arrows in Figs. 1(b)–1(d)]. However, only the negatively refracted beam in Fig. 1(a) has $\mathbf{v}_e\cdot\mathbf{k}<0$, with $\mathbf{k}$ being the fundamental wave vector, and so represents a backwards (left-handed) wave. The "rightness" for the propagating beam can be tested with an appropriately designed scattering experiment on a PC wedged structure. We review the particulars of such wedge design in Sec. IX.

Furthermore, although all dotted beams in Fig. 1 represent umklapp processes, there is a distinct difference between the higher order beams in Figs. 1(b) and 1(c) and the one in Fig. 1(d). In the cases of Fig. 1(b) and 1(c), the $k_\parallel$ of the incident beam falls within the limits of the first BZ (brown hexagon in Figs. 3 and 4). On the other hand, in the case of Fig. 1(d), the $k_\parallel$ of the incident beam falls outside the limits of the first BZ (brown hexagon in Fig. 5). Umklapp processes of the second kind (Fig. 5) can occur also in 1D gratings structure.[14,31] However, umklapp processes of the first kind (Figs. 3 and 4) are specific to certain cases in 2D PCs. As a matter of fact, the origin of their occurrence lies in the arrangement of the reciprocal lattice vectors in the entire 2D space. As a result of this arrangement is that the projection of the modes onto the interface have a periodicity $2\pi/b_{per}$. Nonetheless, the latter quantity does not represent a recipro-

cal lattice vector. Owing to this 2D arrangement, a higher-order beam of the first kind will always coexist with a direct refracted (transmitted) beam. This means we observe birefringence in such cases. Incidentally, we cannot observe this type of birefringence in 1D gratings. In a corresponding case of a 1D layered medium—i.e., with the interface along a symmetry direction[31] and with one band corresponding to the frequency of the incoming wave—we can have at most one refracted beam. We note that hybrid effects between first- and second-kind refractive processes can also occur. It is anticipated that interesting higher-order effects of the first kind can be seen in 3D PCs.

The birefringent effects of the kind in Figs. 3 and 4 are different from the ones observed experimentally by Kosaka *et al.*[15] In the latter study, two different bands were involved for the frequency of the incoming wave. When multiple bands exist for a certain frequency, the procedure we just described in detail must be repeated for each separate band. Many more beams can propagate in these cases. In the case where the relevant bands have different band slope sign, one can observe the simultaneous propagation of beams with different "rightness." The same is true when one band is involved but frequency falls into a band region that is nonmonotonic. We note that Born and Wolf[8] (as well as Yariv and Yeh[47]) adopted an effective medium approach to describe the 1D layered medium. They found that it behaves effectively as a homogeneous medium with optical anisotropy. Therefore, the 1D layered medium is capable of showing birefringent effects. They termed these effects as "form" birefringence to stress the fact that these originate from anisotropy on a much larger scale than the molecule. In optically anisotropic materials, the tensor property of the permittivity introduces two solutions for the dispersion relation (ordinary and extraordinary). The two different dispersion relations give two different equifrequency surfaces in the wave vector space and lead to the familiar birefringent phenomena in these media. In a way, we can say that multifringent phenomena in PCs arising from multiple bands appear for similar reasons as the ones in the optically anisotropic materials. In essence, multiple bands imply multiple dispersion relations for a certain frequency region and, therefore, multiple EFSs within the first BZ, although all EFSs may be extraordinary (noncircular). As we discussed in the preceding paragraph, the birefringent effects of Figs. 3 and 4 have, however, a totally different origin. In these cases, there is a single band for the operation frequency—i.e., a single branch for the dispersion relation—and, therefore, a single EFS in the first BZ. The two beams arise because the modes, represented by the EFS, repeat themselves periodically in the wave vector **k** space. In other words, the periodicity of the PC lattice comes into play in two different ways as far as birefringent effects are concerned. It introduces the possibility of having multiple dispersion relations within the first BZ for a certain frequency region, as in the case of Kosaka *et al.*[15] On the other hand, the periodicity causes the modes to repeat themselves in reciprocal space. The latter is responsible for the beam doubling effects we observed in Figs. 1(b) and 1(c).

A last point we would like to consider concerns the relation between the existence of multiple beams in the medium of incidence and inside the PC. This point has not been addressed despite previous studies regarding the existence of multiple beams in the medium of incidence and the medium succeeding the PC slab and their relation to the transmission properties.[33] Incidentally, Luo *et al.*[3] state that the condition necessary to obtain single-beam propagation inside the PC is $\omega \leqslant 0.5 \times 2\pi c/a_s$, where a_s is the interface period. The quoted condition can be rewritten as $\tilde{f} \leqslant a/2b_{per}$, with b_{per} given by Eq. (R1). In fact, if EM waves are incident in the PC slab from air, this condition guarantees the absence of any higher-order Bragg reflected beams for *any* angle of incidence for cases which are subject to a phase matching condition according to Eq. (1) (see the Appendix, part 1). For a triangular lattice cut along ΓM, this condition becomes $\tilde{f} \leqslant 0.289$. However, FDTD simulation results that we present in the following show this condition *does not* guarantee single-beam propagation inside the PC medium. We consider the case of dielectric rods with permittivity $\epsilon = 60$ and radius $r = 0.37a$. This is a case qualitatively similar to that of Fig. 1(b) (Fig. 3), but with a much lower relevant frequency ($\tilde{f} = 0.275$). We stress that one band only corresponds to this operation frequency. Evidently $\tilde{f} = 0.275$ is below the quoted limit, which means no higher-order Bragg reflected beams exist for any angle of incidence. Indeed, in Fig. 6 we observed only one reflected beam. Notice, however, the clear presence of two propagating beams (solid and dotted arrow). The second beam (dotted arrow) is a higher-order beam of the first kind, like the one shown in Fig. 1(b).

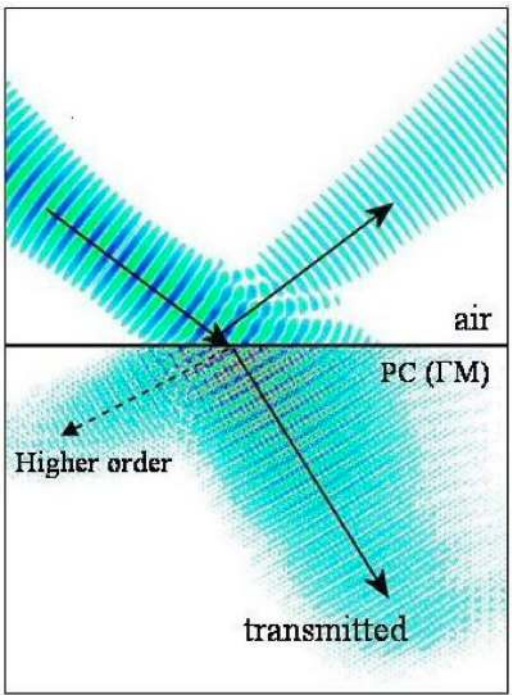

FIG. 6. (Color online) Oblique incidence at the photonic crystal slab with $\epsilon = 60$, $r = 0.37a$, for frequency $\tilde{f} = 0.275$ that is below the Bragg condition for no additional reflected beams for any angle of incidence. Notice that despite the presence of only one reflected beam, there are two propagating beams indicated by the black solid and dotted arrows, respectively.

A single-beam propagation condition cannot be derived always in a simple manner, and one should, in general, carefully examine the wave vector diagrams in the repeated zone scheme. When after the folding process only a sole wave vector in the first BZ gives a causal FB wave, only then do we have single beam propagation. Consequently, the presence of only a single reflected beam is neither a prerequisite nor does it guarantee the presence of a single-beam coupling to the PC medium. Also, note in Fig. 1(d) the clear presence of a higher-order reflected beam, while there is only one propagating beam. For certain simple cases of square and triangular PCs with isotropic EFSs, we will discuss the conditions for single beam propagation in Sec. VI.

IV. FLOQUET BLOCH WAVE AND PHASE VELOCITY

Consider the magnetic field of an *H*-polarized wave inside a two-dimensional periodic photonic crystal structure for the case of *H* (TE) polarization:

$$\mathbf{H}(\mathbf{r},t) = \frac{1}{\sqrt{A_{WS}}} e^{i\mathbf{k}\cdot\mathbf{r}} \sum_{\mathbf{G}} H_{\mathbf{G}}(\mathbf{k},\omega_{n,\mathbf{k}}) e^{i\mathbf{G}\cdot\mathbf{r}} e^{-i\omega_{n,\mathbf{k}}t}\,\hat{z}. \tag{4}$$

A_{WS} is the area of the Wigner-Seitz cell, $\hat{z}$ is the unit vector in the direction out of the plane of periodicity (i.e., the direction of the cylindrical rods), and $\mathbf{G}$ is a reciprocal lattice vector. The coefficients $H_{\mathbf{G}}$ are determined from the eigenvalue equations obtained from the PWE method.[42–44] Apparently the above expression for the field satisfies the Floquet-Bloch theorem[40] for a periodic medium. A wave that propagates according to expression (4) is known as a Floquet-Bloch wave[10,40] with $\mathbf{k}$ lying in the first zone. Any attempt to express the propagation solution in terms of wave vectors $\mathbf{k}'$ lying outside the first BZ results in an expression equivalent to Eq. (4) (see the Appendix, part 2). So the wave vector chosen in the first zone is what characterizes a propagating FB wave. We call this the fundamental wave vector.[10,41] Hence the term "equivalent points" describing points in $\mathbf{k}$ space separated by a reciprocal lattice vector. This property of the FB wave explains the general recipe that we followed in the preceding section to determine the propagating waves. Clearly in the 2D periodic system, all plane wave components contributing to the FB wave with fundamental wave vector $\mathbf{k}$ [expression (4)] propagate together, not separately, with a common energy velocity $\mathbf{v}_e$. Note that no individual plane wave components serve as a separate solution of Maxwell's equations. As a result we do not see clear phase fronts, but rather have phase-like fronts with a "wiggly" profile (see, for example, the FDTD simulation presented in Fig. 1). This type of profile manifests a strong plane wave component mixing[1] present in PC crystals with high-refractive-index modulation.

The questions of how one should approach the subject of defining a phase velocity for the FB wave is still unanswered. What would really be the physical meaning for such definition. Yariv and Yeh[25] defined a phase velocity for a 1D periodic system (see the Appendix, part 3). Equivalently, for the two-dimensional system this definition would be

$$\mathbf{v}_p = \frac{\omega}{K_0^2}\mathbf{K}_0, \tag{5}$$

with $\mathbf{K}_0 = \mathbf{k} + \mathbf{G}_0$ being the plane wave component that has the larger amplitude $H_{\mathbf{G}_0}$ in expression (4). In other words, it is the wave vector of the predominant plane wave component. Many PC studies[27,47,48] focused on the long-wavelength limit, where such a definition would be appropriate.[25] Nonetheless, the interesting refractive behavior of the photonic crystal reveals itself in the higher bands. Unavoidably, the subject of phase velocity in the photonic crystal requires some rethinking. As a matter of fact, Notomi,[1] as well as Kosaka *et al.*,[26] defined a phase index that corresponds to the fundamental wave vector within the first BZ of the FB wave. Accordingly, the phase velocity would be

$$\mathbf{v}_p = \frac{\omega}{k^2}\mathbf{k}, \tag{6}$$

where $\mathbf{k}$ is in the first BZ.

There is an apparent contradiction between these two definitions as given by expressions (5) and (6), respectively. To investigate for the physical meaning of the phase velocity in a periodic medium, we will study numerically the field patterns of the propagating wave in the next section.

V. NUMERICAL DETERMINATION OF THE PHASE VELOCITY

We consider two cases of almost isotropic EFSs. In both cases the fundamental wave vector of the propagating FB wave is chosen to lie along a symmetry direction. We choose again the structure of Notomi [i.e., the same structure as in Fig. 1(a)] and two frequencies (a) $\omega_1 = 0.58\ 2\pi c/a$ lying in a band with negative slope and (b) $\omega_2 = 0.48\ 2\pi c/a$ lying in a band with positive slope. In order to extract information about the phase velocity in the system, we need to compare the time-independent fields at various points along the propagation direction. This methodology is analogous to the one followed by Ziolkowski and Heyman,[49] where the negative phase index was numerically confirmed for a homogeneous slab material with $\epsilon = -1$ and $\mu = -1$.

For this purpose, we consider a pulsed signal $f(t)\cos(\omega_0 t)$ with

$$f(t) = \begin{cases} 0 & \text{if } t < t1, \\ \dfrac{(t-t1)^2}{\alpha^2 + (t-t1)^2} & \text{if } t1 < t < t2, \\ \dfrac{(t-t3)^2}{\alpha^2 + (t-t3)^2} & \text{if } t2 < t < t3, \\ 0 & \text{if } t > t3. \end{cases} \tag{R2}$$

The parameters are chosen to give a broad pulsed signal in time with a small $\delta\omega$ around the operation frequency ω_0. For operation frequency ω_1 the parameters are $\alpha = 21.9$ T, $t1 = 19.6$ T, $t2 = 499.7$ T, and $t3 = 979.9$ T. For operation frequency ω_2 they are $\alpha = 18.1$ T, $t1 = 16.2$ T, $t2 = 413.6$ T, and $t3 = 810.9$ T. The period T of the EM wave is different for the two cases, and the parameters are chosen to correspond to

the same actual time. The pulse is launched normally to the photonic crystal structure with an interface cut along the ΓK symmetry direction. We monitor the magnetic field $\mathbf{H}$ for each time step for a long time for certain points along the propagation direction. We refer to these points as detector or sampling points. The Fourier transform of the time series $\mathbf{H}(y,t)$, where y is the coordinate of a detector point, yields the corresponding amplitude $\mathbf{H}(y,\omega)$.

Before we proceed with our analysis, we should mention that in order to make any assessment regarding the phase velocity the field patterns inside the slab should be as close as possible to the infinite system patterns given by the FB wave expressed in Eq. (4). For this purpose, our structure should emulate a semi-infinite PC slab. Any wave that couples to the slab will undergo multireflections between the two interfaces. In order to achieve our goal—i.e., a structure acting similar to a semi-infinite slab—we must somehow eliminate or reduce substantially the amplitude of any reflected beam originating from the second interface. For this purpose, we consider a periodic structure consisting of 30 sites along the lateral direction and 100 rows along the propagation direction. Of these 100 rows, 30 rows consist of rods with dielectric constant 12.96 embedded in air. This part of the structure is the area of concentration. We take detector points that monitor the field as a function of time in this area. In the remaining 70 layers, we introduce absorption (both in the sites and in the background) so that the field is attenuated before exiting the crystal. We introduce electric and magnetic conductivity (σ_e and σ_m, respectively) to each numerical cell, so that the impedance of the each grid cell in the absorptive layer would be the same as the corresponding one in the nonabsorptive layer. It is equal to $\sqrt{\mu_0/\epsilon_0\epsilon_{i,j}}$, where ϵ_0 and μ_0 are the vacuum permittivity and permeability, and $\epsilon_{i,j}$ is the relative permittivity of the 2D grid cell located at the point with grid coordinates (i,j). This is possible when the conductivities that we introduced follow the relations $\sigma_e = \epsilon_{i,j}\sigma_0$ and $\sigma_m = (\mu_0/\epsilon_0)\sigma_0$, where σ_0 is a conductivity parameter. If the parameter σ_0 is chosen very low $(10^{-5}\ \Omega^{-1}\ \mathrm{m}^{-1})$, the reflections of the beam when entering the absorptive layer are low. In order to make a rough estimate of the EM wave energy that gets reflected back to the nonabsorptive layer where we monitor the fields, we look at the attenuation profile of the fields inside the absorptive layer. In addition, reflections can occur when the EM wave meets the absorptive boundary. To check these, we considered oblique incidence. Overall, we find the amplitude of the field that gets reflected back into the nonabsorptive layer is about 10% of the amptitude of the refracted EM wave.

The set of points that serve as detectors are chosen normal to the surface, which coincides with the propagation direction $\hat{y}$, chosen along the ΓM symmetry direction. Their respective locations are a distance $b=\sqrt{3}a$ apart, essentially the periodicity for the propagation direction. We take the Fourier transform of the time series representing the evolution of the magnetic field at a certain point.[50] Afterward, we calculate the ratios $H(\omega,d_{i+1})/H(\omega,d_i)$. ω represents the frequency of the input pulse train and d_i the location of the ith detector point. Since the distance between the detectors is one period along the propagation direction, this ratio should be equal to $\exp(ikb)$, with k restricted to the first BZ. Therefore, by studying the field patterns, we can extract information about the phase velocity, defined in accordance with Notomi[1] [expression (6)].

We calculate the field ratio at adjacent detector points and extract the wave vector from the formula

$$k_i = \frac{1}{ib}\ln\frac{H(\omega,d_{i+1})}{H(\omega,d_i)}, \tag{7}$$

where i stands for the ith detector point. Notice that the Fourier-transformed fields are complex and therefore the logarithmic function is complex and multivalued. We record all possible values with the real parts falling inside the first BZ. Taking the average for the various detector points for the case of $\omega=\omega 1$, we find that two possible solutions exist for k: (1) $k=(1.47+0.005i)a^{-1}\pm(0.01+0.008i)a^{-1}$ and (2) $k=(-2.16+0.005i)a^{-1}\pm(0.01+0.008i)a^{-1}$. In order to choose the correct solution, we further study the field patterns. We also consider the ratio of two observation points located around the middle of the 30-cell PC layer, separated by $\Delta y = b/31$. The field ratio determined by the FDTD simulation is $3.05-0.63i$. Now we calculate the same ratio theoretically with the PWE expansion method[42–44] for the two possible wave vector solutions determined from Eq. (7). Using solution (1) for the wave vector (real part only) in PWE we obtain a field ratio of $4.3+2.3i$. For the second solution, we obtain a field ratio of $2.98-0.52i$. Apparently only solution (2) gives a ratio that agrees well with the FDTD results. We note that in order to eliminate any discrepancies resulting merely from the discretization, we used in the PWE the actual numerical dielectric grid used in the FDTD. However, there is still a small discrepancy between the PWE field ratio and numerical FDTD ratio that may stem from a combination of the following—angle span of incident source, Fourier transform zero padding errors, reflections from absorptive boundary layer, etc. This is the same reason for which a small imaginary part is present in the wave vector value. Also note there exists some ambiguity associated with the exact location of the first interface, since we are dealing with a periodic medium.[32] In the boundary layer the field values may deviate from the values given by the FB wave expression [Eq. (4)]. Therefore, we place the first detector point at the center of the second row of cylinders and assign $d_1=0$.

In the analysis above we used the FDTD field patterns in the "semi-infinite" slab to determine that the wave vector inside the photonic crystal for the case with frequency $\omega=0.58\times 2\pi c/a$ is $k=-2.16a^{-1}$. This value is in good agreement with the corresponding value from an EFS analysis $(k=-2.48a^{-1})$ (see Ref. 51). Expression (6), with the use of the wave vector obtained from the field pattern analysis, gives $\mathbf{v}_p\sim -1.69c\hat{y}$ (c being the velocity of light). Following the same procedure but for the case with frequency $\omega_2 = 0.48\times 2\pi c/a$, we calculate a phase velocity $\mathbf{v}_p\sim 2.23c\hat{y}$. In both cases, we determined the magnitude and the sign of the phase velocity. The field pattern analysis for a semi-infinite slab gives a negative phase velocity (i.e., opposite to the propagation direction) for the case with frequency $(\omega_1 = 0.58\times 2\pi c/a)$. This result implies that the "rightness" of

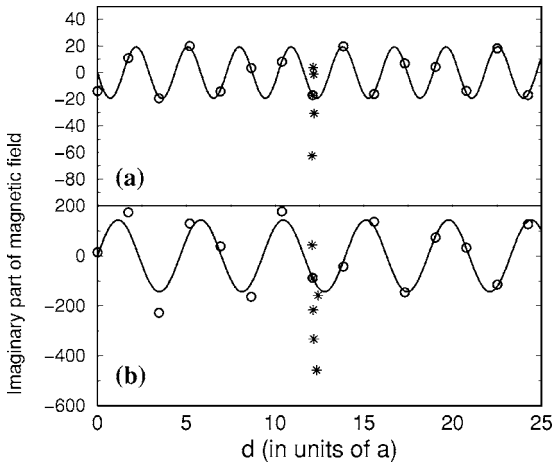

FIG. 7. The open circles represent the imaginary part of the Fourier transformed magnetic field, sampled in time at different points along the propagation direction, y_i. The sampling points are separated by one period along the propagation direction which is the ΓM direction. PC has rods with $\epsilon=12.96$ and radius $0.35a$, and the magnetic field lies along the cylinders (H polarization). In both cases, the corresponding equifrequency surfaces are almost isotropic. Top panel (a) is for $\tilde{f}=0.58$, which belongs to a band with negative slope. The bottom panel is for $\tilde{f}=0.48$, which belongs to a band with positive slope. The solid lines are $\propto\sin(ky_i)$, where k is the real part of the numerically calculated wave vector. Thus, $k=-2.16a^{-1}$ for case (a) and $1.35a^{-1}$ case (b). The stars represent the imaginary part of the Fourier-transformed magnetic field for points in the neighborhood of $y_i=7b$, with $b=\sqrt{3}$.

the propagating beam is negative in this case. So a field pattern analysis with the FDTD method for a semi-infinite slab confirms the results we obtained from the wedge simulation experiment.[5] We will discuss more about the "rightness" of propagation in Sec. IX.

In order to visualize the physical meaning for the phase velocity defined in Eq. (6) we plot the imaginary part of the magnetic field $H(\omega)$ for various detector points. We show the results for both cases with frequencies ω_1 and ω_2 in Figs. 7(a) and 7(b), respectively (open circles). The solid line is $A\sin ky$ where k is the wave vector as determined from the field pattern analysis above and y is the distance from the first detector point. The amplitude A is determined by fitting to the numerical value of the imaginary part of the field at $y=7.0b$, with $b=\sqrt{3}a$. Moreover, we choose an additional set of detector points, closely spaced and around the middle of the 30-row PC layer. We indicate the imaginary part of the corresponding Fourier transformed field of these points with stars in Fig. 7. We see that the solid sinusoidal line passes closely to the field values corresponding to the first set of detector points (circles). However, the field values for the second set of detector points (stars) deviate substantially from the sinusoidal line and show very high variations. This is evidence of the strong mixing between the plane wave components contributing to the FB wave in expression (4).

From the FB wave expression we obtain (see the Appendix, part 4)

$$\langle H(\mathbf{r}=\mathbf{R})\rangle = e^{i(\mathbf{k}\cdot\mathbf{R}-\omega t)}\langle H(\mathbf{r}=0)\rangle, \tag{8}$$

where $\mathbf{R}$ is a Bravais lattice vector and $\langle\cdots\rangle$ the spatial average within the unit cell. All detectors points of the first set are Bravais lattice vectors along the ΓM symmetry direction. Our numerical results shown in Fig. 7 together with expression (8) suggest that the phase velocity describes how fast the phase of the EM wave travels from period to period in the PC lattice. However, information of how fast the phase travels between adjacent points cannot be determined. Thus, it is clear why it is necessary to fold the wave vector in the first zone and define the phase velocity as in expression (6). We will return to the same subject and the appropriateness of definition (5) when we discuss photonic crystals with low-index modulation in Sec. X.

VI. EFFECTIVE PHASE INDEX

It is desirable to define an effective phase index that is correlated with the phase velocity as defined in Sec. IV with Eq. (6). Correspondingly,

$$\mathbf{v}_p = \frac{c}{|n_p|}\hat{k}. \tag{9}$$

The sign of n_p is chosen to reflect the left- or right-handed behavior of the PC system[5] and in accordance with the left-handed literature.[16] This definition for the index is consistent with the analysis by Notomi.[1] However, we have seen in Secs. II and III that the photonic crystal system can be quite complicated and various higher-order effects may arise under certain conditions. One must bear in mind all these effects when interpreting the effective index for the photonic crystal system. Next, we analyze what this index represents, as well as what properties can be inferred from this index.

Let us consider a Snell-like formula

$$\sin\theta_{inc} = n_p \sin\theta_{ref}, \tag{10}$$

for EM waves incident from air, into a PC medium with phase index n_p (in general depends on the refracted angle θ_{ref}). Sometimes, it is assumed that Snell's formula gives the direction of the propagating wave. This is not true, because, in general, in the photonic crystal the direction of the refracted wave vector and the direction of the propagating signal do not coincide. We discussed this in Sec. III. Note, again, that the direction of propagation is always the direction of the energy velocity $\mathbf{v}_e$. Nevertheless, provided that certain conditions apply, there will be only a single refracted beam in the photonic crystal, which propagates with an angle given by Snell's formula [Eq. (10)]. We determined these conditions for the special case of 2D triangular and square PC lattices. They are the following.

(i) Interface cut along a symmetry direction of the crystal.

(ii) An almost isotropic equifrequency contour.

(iii) $\mathbf{k}_{inc\|}$ falling between $-\pi/b_{per},\ldots,\pi/b_{per}$.

(iv) $|n_p|<1/(2C_{str,cut}\tilde{f})$, with b_{per} given by (R1) and

$$C_{str,cut} = \begin{cases} 1 & \text{for triangular cut along } \Gamma K, \\ \sqrt{3} & \text{for triangular cut along } \Gamma M, \\ \sqrt{2} & \text{for square cut along } \Gamma M, \\ 0 & \text{for square cut along } \Gamma X. \end{cases} \quad \text{(R3)}$$

Cases with slanted interfaces are subject to a rather complex phase matching conditions.[34] As a matter of fact, higher-order waves are more likely to occur in such cases, hence the first condition. The second condition guarantees that $\mathbf{v}_e$ and $\mathbf{k}$ are about coaxial. This implies that the angle derived from Snell's formula represents the propagating angle. The third condition guarantees that the refracted wave is not a higher-order wave (specifically of the second kind as described in Sec. III). If the wave is a higher-order wave of the second kind and the EFS is isotropic, it will propagate with an angle that may be opposite in sign to the sign of the effective index. Finally, the last condition, in combination with the first and second conditions, guarantees the absence of higher-order waves of the first kind for any angle of incidence; i.e., it guarantees single-beam propagation. However, if we desire a single reflected beam as well, then the condition (see the Appendix, part 1),

$$\theta_{inc} < \theta_{lim} = \sin^{-1}\left(\frac{a}{\tilde{f} b_{per}} - 1\right), \quad (11)$$

with $\tilde{f} < a/b_{per}$, should also be observed. Notice that if $\tilde{f}$ exceeds the value of a/b_{per}, then higher-order reflected beams occur for any angle of incidence.

Even in the absence of condition (iii), if the rest of the conditions are valid we still obtain single-beam propagation. In this case, a modified Snell-like formula can be used to determine the single refracted beam,

$$\sin\theta_{incp} = n_p \sin\theta_{ref}, \quad (12)$$

where

$$\theta_{incp} = \sin^{-1}\left(\sin\theta_{inc} - \frac{ma}{\tilde{f} b_{per}}\right) \quad (13)$$

and m chosen so that $|\sin\theta_{inc} - ma/(\tilde{f} b_{per})| < \min(1, a/(2b_{per}\tilde{f}))$.

To summarize the purpose of defining an effective index is that it gives qualitative and/or quantitative insight into the PC properties such as the magnitude and direction of the wave vector, the "rightness" of the medium conveyed in the sign of the index, and, under certain conditions, the energy velocity. However, caution should be taken by the use of such a phase index. It does not contain information about higher-order beams that can couple inside the crystal or in the air medium (reflected beams) or both. A wave vector diagram type of analysis always offers a more complete treatment for the system. We also alert the reader that in no way should this phase index be used in Fresnel-type formulas[9] to determine the transmission and reflection coefficients of an EM wave incident on the PC structure.

VII. ENERGY AND GROUP VELOCITY

We have seen in Ref. 5 that the sign of the product $\mathbf{v}_e \cdot \mathbf{k}$ serves as a theoretical prediction for the sign of the "rightness" for the PC system. Such theoretical predictions agree well with the FDTD wedge simulation results.[5] We used the equality between the energy velocity and the group velocity to easily identify the frequency regions with negative "rightness."[5] These would be the regions that correspond to a band with negative slope. In Ref. 33 the equality between group and energy velocity is shown for 3D periodic dielectric structures. We verified that such equality holds in our 2D photonic crystal as well. In order to show this, we derive expressions for both the group velocity $\mathbf{v}_g$ and energy velocity $\mathbf{v}_e$. Both expressions are in terms of the FB wave coefficients.

For the energy velocity we start with the respective definition[52]

$$\mathbf{v}_e = \frac{\langle \mathbf{S} \rangle}{\langle U \rangle}, \quad (14)$$

where the brackets $\langle \cdots \rangle$ refer to the spatial average within the unit cell of the time-averaged quantities. $\mathbf{S}$ is the Poynting vector, and U is the energy density. Then we calculate both the Poynting vector and energy density with the use the FB wave expression (4), and Maxwell's equations. We then calculate the averages within the unit cell by taking into account appropriate normalization conditions. For the group velocity we follow the $\mathbf{k} \cdot \mathbf{p}$ perturbation formalism for PC systems.[53–55]

We find identical expressions for both the group and energy velocity for both polarizations. In particular we get, for the H (TM) polarization (magnetic field along the rods) (Ref. 56),

$$\mathbf{v}_e = \mathbf{v}_g = \frac{c^2}{\omega_{n,\mathbf{k}}} \sum_{\mathbf{G}_1,\mathbf{G}_2} (\mathbf{k} + \mathbf{G}_1)\, \eta_{\mathbf{G}_1,\mathbf{G}_2} H_{\mathbf{G}_1}(\mathbf{k}, \omega_{n,\mathbf{k}}) H_{\mathbf{G}_2}(\mathbf{k}, \omega_{n,\mathbf{k}}) \quad (15)$$

and, for the $\mathbf{E}$ (TM) polarization (electric field along the rods),

$$\mathbf{v}_e = \mathbf{v}_g = \frac{c^2}{\omega_{n,\mathbf{k}}} \sum_{\mathbf{G}} (\mathbf{k} + \mathbf{G}) E^2_{\mathbf{G}}(\mathbf{k}, \omega_{n,\mathbf{k}}). \quad (16)$$

Evidently, the energy velocity for our 2D photonic crystal can be calculated with the use of formulas (15) and (16) for the H and E polarization cases, respectively. One needs to know the fundamental wave vector, the index of the band of interest, and the FB wave coefficients ($H_{\mathbf{G}}$ and $E_{\mathbf{G}}$, respectively). The latter are determined easily from the PWE method.[42–44]

VIII. GROUP REFRACTIVE INDEX

A group index n_g can be defined[5] in accordance with the traditional waveguide and optical fiber literature:[57]

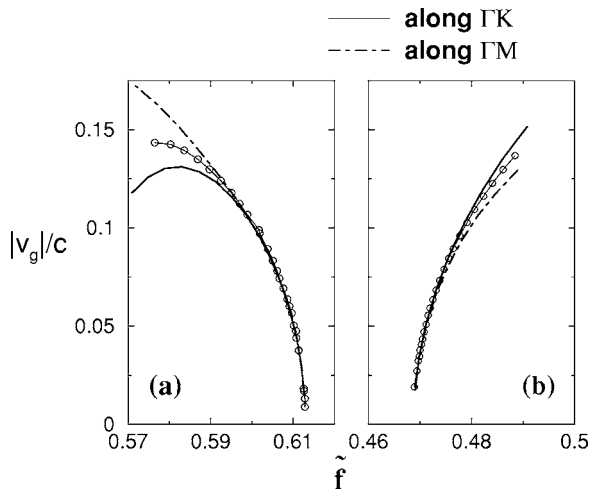

FIG. 8. Magnitude of the group velocity for cases with almost isotropic EFS for a photonic crystal of rods with $\epsilon=12.96$ and radius 0.35, for H polarization. In (a) the results of the fifth band (negative-slope band) are shown. In (b) the results of the fourth band (positive-slope band) are shown. The solid and dot-dashed lines represent the results from the $\mathbf{k}\cdot\mathbf{p}$ perturbation method for signal along the ΓK and ΓM directions, respectively. The solid lines with circles represent the results obtained when considering the system having an effective phase index n_p. The index is calculated from the band structure (EFS) and is frequency dependent. Agreement between the two results is excellent close to the band edge. Since the anisotropy increases as one moves away from the band edge, so does the discrepancy between the two values.

$$|n_g| = \frac{c}{|\mathbf{v}_g|}. \tag{17}$$

For a PC structure with the same parameters as the one in Fig. 1(a), we calculated the group velocity vector for the fifth band (band with negative slope) and the fourth band (band with positive slope) for a range of frequencies where the EFS contours are "almost" isotropic. We used the $\mathbf{k}\cdot\mathbf{p}$ perturbation method[53–55] result given in expression (15). The results for the magnitude of the group velocity are shown in Fig. 8 for both bands and both symmetry directions (ΓM and ΓK). Notice that the closer to the band edge, the better the agreement between the group velocities for the two symmetry directions. This is expected, since the degree of anisotropy increases as one moves away from the band edge. Alternatively, we can consider the PC as an isotropic system with effective dispersive phase index $n_p(\omega)$. In this case,

$$|\mathbf{v}_g| = \frac{c}{|n_g|}, \tag{18}$$

with

$$n_g = |n_p| + \omega\frac{d|n_p|}{d\omega}. \tag{19}$$

We also show in Fig. 8 the results obtained from formulas (18) and (19) for comparison. Because of the small anisotropy in the EFS shape, we use for n_p the average value of the two symmetry directions. For both bands the results given from Eqs. (18) and (19) are shown as a solid line with circles. We see that the results from expression (18) are in very good agreement with the corresponding ones calculated from the $\mathbf{k}\cdot\mathbf{p}$ perturbation method. This is especially true for frequencies very close to the band edge. So, in the cases that conditions (i)–(iv) of Sec. VI are satisfied, expression (18) [with the use of Eq. (19)] provides a good estimate for the group and energy velocity of the single transmitted beam.

The sign of the group index manifests the sign of refraction at the air-PC interface. As in the case of the phase index n_p, though, caution must be exercised with the use and interpretations of the group index. We stress that the sign n_g relates only to the sign of refraction for the transmitted beam. It does not contain any information for higher-order waves that we discussed in Sec. III.

IX. THE "RIGHTNESS' OF THE PC SYSTEM: DESIGNING THE WEDGE-TYPE EXPERIMENT

We observed different negative refraction effects shown in Fig. 1 in Sec. I. It is important to be able to characterize the nature of propagation (left-handed or not) for the finite PC structure. In Ref. 5 we found that the presence of a negatively refracted beam does not necessarily imply left-handed behavior. We confirmed[5] that indeed the sign of the "rightness" follows the theoretical prediction for the sign of n_p from the band structure. A wedge type of experiment that can determine unambiguously the PCs "rightness" can be designed in most cases. However, in Sec. III we observed different higher-order effects that can potentially complicate the interpretation of such an experiment. So, when we think of the wedge experiment, we attempt to eliminate as much as possible the presence of multiple beams. This way we can make an unambiguous assessment for the "rightness" of the system. Therefore, it is important to take into consideration the symmetry properties of the crystal, as they reveal themselves in the cuts of the interfaces and in the eigenmodes in $\mathbf{k}$ space for the frequency of operation. We review the intricate details of the wedge design for the different PC cases in the following.

The wedge separates the space into three different areas as shown in Fig. 9: the area where the fields come from (area 1), the area inside the wedge (area 2), and the area after the fields experience scattering (area 3). Choosing the interfaces of the wedge in an arbitrary direction implies coupling of a high number of beams both in areas 2 and 3. Thus, we choose both interfaces of the wedge along a symmetry direction. From now on we will refer to a certain wedge design as (sym1)-(sym2) where sym1 is the symmetry direction of the first interface, while sym2 is the symmetry directions of the second interface. For square and triangular PCs, if the wedged interface is along a symmetry direction, then we can apply the phase matching condition on interface ($I2$) to determine the outgoing beams in area 3.[5] Correspondingly we get

$$\theta_{out,m} = \tan^{-1}\frac{\mathbf{k_t}\cdot\hat{\mathbf{w}} + \dfrac{2\pi m}{b_{per}}}{k_{\perp,m}}, \tag{20}$$

for m that satisfy the condition

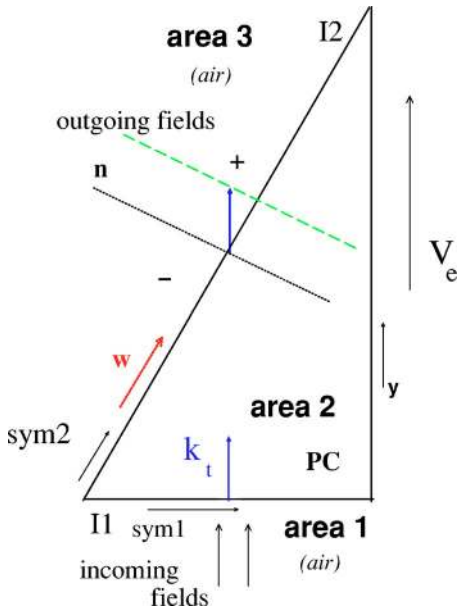

FIG. 9. (Color online) A general case of the PC wedge experiment is shown diagrammatically.

$$k_{\perp,m}^2 = \frac{\omega^2}{c^2} - \left(\mathbf{k_t}\cdot\hat{\mathbf{w}} + \frac{2\pi m}{b_{per}}\right)^2 > 0. \qquad (21)$$

The outgoing angles $\theta_{out,m}$ in area 3 are measured from the normal to the wedge. $\mathbf{k}_t$ is the fundamental wave vector of the FB wave that couples to area 2. Finally, $\hat{w}$ represents a unit vector along the wedged interface and b_{per} is given by Eq. (R1). We show diagrammatically a general case of the wedge experiment in Fig. 9. If the PC is right handed, then the wave vector does not flip sign when crossing the interface since $\mathbf{v}_e\cdot\mathbf{k}>0$. In that case $\mathbf{k}_t\cdot\hat{\mathbf{w}}$ is positive. Correspondingly for a left-handed PC $\mathbf{k}_t\cdot\hat{\mathbf{w}}$ becomes negative. The sign of the quantity $\mathbf{k}_t\cdot\hat{\mathbf{w}}$ determines the sign of the outgoing angle with $m=0$. In other words, the location of the zeroth-order outgoing beam in area 3 determines the "rightness" of the PC. To have an unambiguous interpretation of the result we can study only cases with only one outgoing beam. We can make still reliable conclusions if we have at most one higher-order wave in area 3, with magnitude quite different from the zeroth-order outgoing beam. In such cases we would also need an estimate for the magnitude of the transmitted wave vector. This knowledge can be obtained from the PWE method[42–44] for the infinite system. We stress, though, that in any case the "rightness" for the PC from such a simulation experiment is determined independently and no information regarding this quantity is borrowed from the infinite system analysis.

For triangular lattice, we identify two general classes: those with "almost" isotropic EFS and those with anisotropic EFS (broken curves with sixfold symmetry) in **k** space. Actually, limiting cases between these two classes exist. However, their respective frequency range is generally quite small. Evidently, some *a priori* general knowledge for the system is necessary before designing and/or interpreting the wedge simulation experiment. This knowledge can be extracted from the band structure. One locates "almost isotropic cases" at the band edge, where the band structure is bell-shape like. Away from the band edge, anisotropic EFSs are expected, residing close to the the edge of the Brillouin zone.

For triangular lattices with almost isotropic EFS we find the ΓK-ΓK design to be appropriate. We choose ΓK as the symmetry direction of the wedged interface, since higher-order Bragg waves in area 3 start coupling at higher frequencies for that case. Moreover, in higher bands it is very likely a part of the energy to get reflected back inside the PC at the wedged interface. This is a factor that can potentially obscure the wedge experiment. However, if we choose a 60° wedge, the beam resulting in area 3 after consequent multireflections will always be along the normal to the wedge. Thus we also choose ΓK for the first interface as well. For frequencies higher than ~0.56 one should become alert to the possibility of coupling of higher-order Bragg waves in area 3 according to Eqs. (20) and (21). Note that for this class of cases $\mathbf{k}_t\cdot\hat{\mathbf{w}}$ in Eqs. (20) and (21) is equal to $k_t\cos 30°$ with k_t being positive if $\mathbf{k}_t$ points towards $+y$ and negative otherwise. Moreover, at frequencies higher than ~0.75 the interpretation of the results starts becoming vague. Also, caution must be exercised at lower frequencies for cases with $n_p>2/\sqrt{3}$. The EM wave in area 2 experiences total internal reflection for such cases.

We proceed in our discussion with cases that have anisotropic EFS—i.e., broken curves with sixfold symmetry in **k** space. We determine—from a wave vector analysis at the first interface as developed in Sec. III—that there are three different FB waves having different fundamental wave vector $\mathbf{k}_{t,i}$, which couple to area 2. To determine the complete set of outgoing beams in area 3, we need to apply Eq. (20) along with condition (21) for each individual $\mathbf{k}_{t,i}$. One of them $\mathbf{k}_{t,1}$ always lies along the y direction as in Fig. 9. Each of the remaining two lies at an acute angle ϕ with respect to $\mathbf{k}_{t,1}$. The magnitude of the angle ϕ depends on the specific case. Still, even in these complicated cases it is possible to make a clear assessment of the "rightness" with a wedge experiment. We examined many typical cases falling in this category with the wave vector diagram formalism and found ΓM-ΓM to be the suited design. Note that we cannot study cases with a frequency below ~0.50 in order to ensure the coupling of the zeroth-order beam for the central wave vector $\mathbf{k}_{t,1}$ into area 3. In addition, we should not study cases with a frequency above ~0.60. Observing these limits makes it easy to identify clearly the "rightness" of the PC. It will coincide with the location in area 3 of the larger in magnitude outgoing angle.

We show two examples of the wedge experiment simulation representing the two aforementioned categories in Figs. 10(a) and 10(b), respectively. In Fig. 10(a) we show FDTD results for waves incident on a PC wedged structure with the same structural parameters as in the case of Fig. 1(b). In Fig. 1(b) we observed the coexistence of a negatively and a positively refracted beam when the wave refracts on the PC interface. In Fig. 10(a), however, we clearly see one outgoing beam in the positive hemisphere. The second beam around the normal is just the result of multireflections. Thus, the PC is "right-handed" for this case. In Fig. 10(b) we study a case falling in the second class. We located the larger in magni-

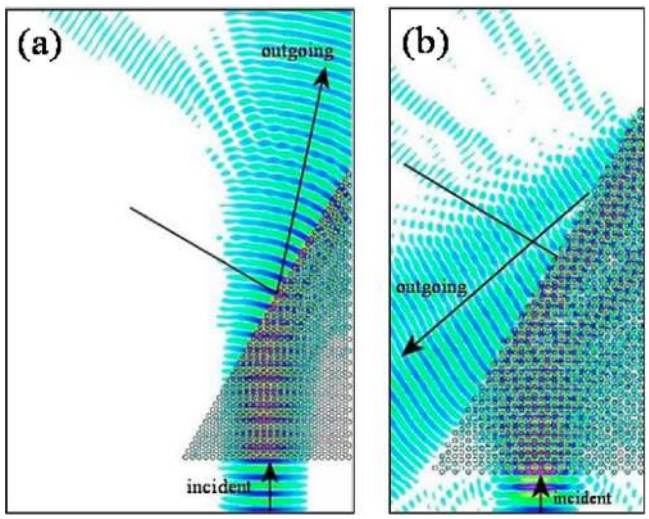

FIG. 10. (Color online) The wedge simulation experiment. (a) FDTD results for the case of Fig. 1(b). A large positive outgoing angle is seen. The second beam is along the normal to the wedge direction and is due to multireflections in the upper part of the wedge. Thus, the PC is right handed. (b) FDTD results for triangular lattice consisting of rod with dielectric constant 12.96 and radius $0.30a$ in air. Magnetic field along the cylinders (H polarization) and operation frequency of $\tilde{f}=0.50$. The outgoing beam with the larger angle is the negative hemisphere. Therefore, the system is left-handed in this case.

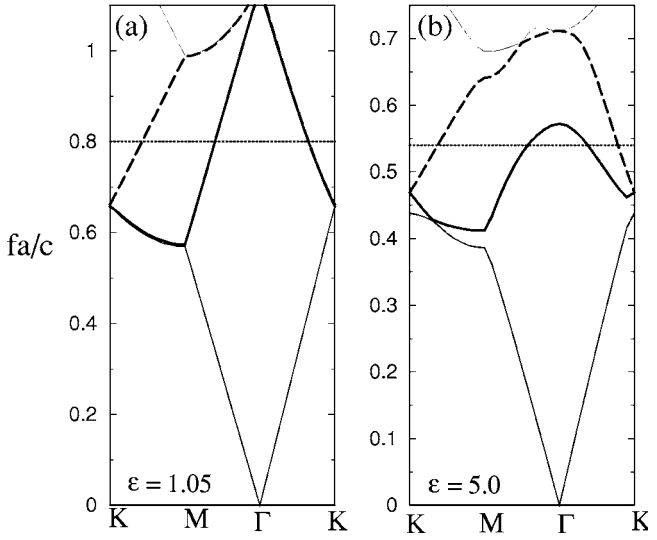

FIG. 11. The band structure for the two limiting cases with $\epsilon=1.05$ and $\epsilon=5.0$. The heavy solid line represents the second band, and the dashed line represents the third band, when folded in the first Brillouin zone. The operation frequency is chosen to be around approximately the middle of the second and third bands, and is indicated in the figure with the dotted line. Note that in (a) the bold dashed line falls on top of the bold solid line along the ΓK direction.

tude angle in the negative hemisphere. Hence, the PC is left- handed in this case. In both cases the results agree with the theoretical predictions for the sign of $\mathbf{v}_e \cdot \mathbf{k}$ made from the band structure.

In designing the wedge experiment for square PC structures, one should take into consideration the same criteria as in the cases of triangular PCs. In this way, we determined that for both classes of cases (isotropic and anisotropic) the appropriate wedge design is ΓM-ΓX. We note that the anisotropic cases we consider for the square lattice have EFSs that are broken curves with fourfold symmetry instead.[3] The anisotropic square cases are not as complex as the triangular ones. Owing to the fourfold symmetry, only one—not three as in the corresponding triangular case—FB wave couples into area 2. For high frequencies, one should be alert for higher-order Bragg couplings, determined from Eq. (20) and (21). Typical anisotropic cases may also suffer from total internal reflection if $\tilde{f}$ is smaller than ~ 0.45. Isotropic cases with $n_p > 2/\sqrt{2}$ should also be avoided for the same reason.

X. HIGH-INDEX vs LOW-INDEX MODULATION

In the previous sections we focused our analysis in describing the propagation properties of EM waves for 2D crystals with high-index contrast between the constituents dielectrics. We have seen different anomalous refractive effects including birefringence. We provided a consistent recipe based on the wave vector diagram and band structure properties of the system, which determines all properties of each propagating beam such as refracted angle, phase, energy velocity, and "rightness." Since the analysis in the preceding section focuses on PCs with high-index modulation, it is important to investigate the limits of validity of our theoretical analysis. We will now examine photonic crystals with low-index modulation in the context of all the aforementioned properties which characterize the propagating beam.

We consider a 2D photonic crystal lattice that consists of dielectric rods in air with radius 0.35 a in triangular arrangement for the H-polarization case. We let the dielectric constant of the rods vary, starting from the value of 1.05 (value close to the dielectric constant of air) and investigate the photonic crystal's response as the dielectric constant of the rods increases. Unavoidably, when the index contrast is low, it is not possible to isolate cases where only one band corresponds to the relevant frequency range. In each case the dielectric constant of the rods, ϵ, takes the following values: (a) $\epsilon=1.05$, (b) $\epsilon=1.2$, (c) $\epsilon=1.5$, (d) $\epsilon=2.0$, and (e) with $\epsilon=5.0$. The operation frequency is chosen to lie approximately in the middle of the spectrum corresponding to the second and third band, as we see in Fig. 11. Therefore, we choose $\tilde{f}=fa/c$ equal to 0.80, 0.78, 0.75, 0.70, and 0.54 for cases (a), (b), (c), (d), and (e), respectively.

We first consider the case with an interface along ΓK. The fields from the FDTD simulation for oblique incidence with angle 8°. are shown in Fig. 12. We notice that in case (a) the wave enters essentially undisturbed inside the PC with the angle of propagation pretty much the same as the angle of incidence. As the index contrast increases, the propagating angle still remains close to 8°, but "wiggly" features start to appear in the phase fronts. Refraction angle remains positive. For index contrast 5.0 [case (e)] we see a beam in the negative direction. With the PWE method we determined that for

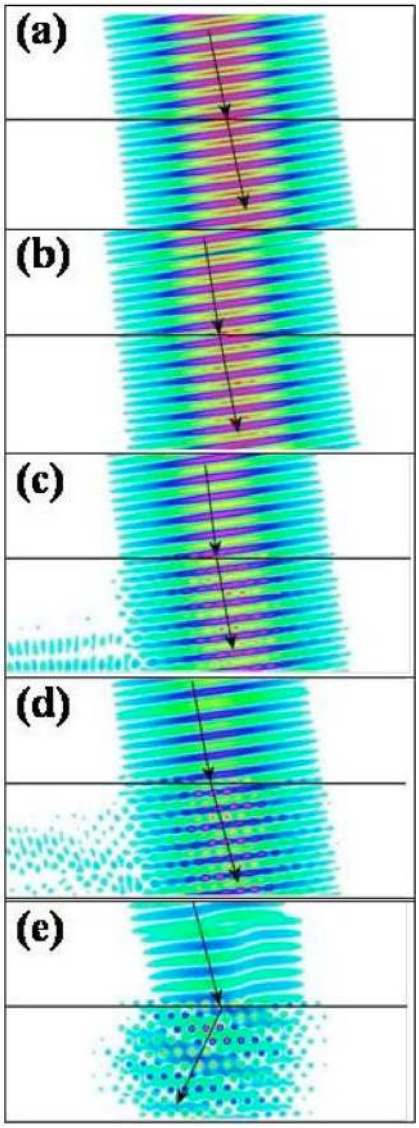

FIG. 12. (Color online) Refraction at oblique incidence with angle of 8° at a PC lattice of rods with radius $0.3a$ for H polarization. We consider a dielectric constant equal to 1.05, 1.2, 1.5, 2.0, and 5.0 for cases (a), (b), (c), (d), and (e) respectively. Positive refraction is seen in all cases except in case (e) where index contrast is high.

the cases (a)–(c) there is mainly one predominant component contributing in the FB wave, given by expression (4). Mixing between the different components in the FB sum starts to appear in case (d) and becomes stronger in case (e).

Suppose that we could describe our periodic system with an effective medium having an effective dielectric constant consistent with Maxwell-Garnett theory[48] and, therefore, an effective index n_{eff} given by

$$\frac{1}{n_{eff}} = \sqrt{\frac{1}{\epsilon} f + (1-f)}. \tag{22}$$

In such a case, the field inside the PC is a plane wave,

$$H(\mathbf{r},t) \sim A e^{i(\mathbf{K}\cdot\mathbf{r}-\omega t)}, \tag{23}$$

with $\mathbf{K}=\mathbf{n}_{eff}\omega/c$.

Alternatively, propagation in our periodic system can be described with an FB wave given by expression (4). However, for cases (a)–(c) we found only one predominant term in the FB expression. Thus,

$$H(\mathbf{r},t) = A e^{i(\mathbf{k}_{pred}\cdot\mathbf{r}-\omega t)} + O(\epsilon^2). \tag{24}$$

$\mathbf{k}_{pred}=\mathbf{k}+\mathbf{G}_0$, with $\mathbf{k}$ being in the first BZ and $\mathbf{G}_0 = 4\pi/\sqrt{3}a^{-1}\ \hat{y}$. Here y is the propagation direction (ΓM in this case). Very good agreement is found between magnitude and direction of $\mathbf{K}$ and $\mathbf{k}_{pred}$ for cases (a)–(c) with low index contrast. Moreover, in these cases the energy velocity has almost the same direction as $\mathbf{k}_{pred}$ and correspondingly $\mathbf{K}$. As a matter of fact, in these cases we get only one surviving term in expression (15) corresponding to $\mathbf{G}_1=\mathbf{G}_2=\mathbf{G}_0$. Thus, the energy velocity becomes

$$\mathbf{v}_e \cong \frac{c^2}{\omega_{n,\mathbf{k}}}(\mathbf{k}+\mathbf{G}_0)\,\eta_{\mathbf{G}_0,\mathbf{G}_0} H^2_{\mathbf{G}_0}(\mathbf{k},\omega_{n,\mathbf{k}}) \propto \mathbf{k}_{pred}. \tag{25}$$

In other words, when the index contrast is very low [cases (a)–(c)], only one component in the FB sum contributes significantly. Then, the direction of the energy velocity is very close to the direction of the predominant wave vector. However, we observed that as more plane wave components contribute in the FB sum, the directions of the predominant wave vector and energy velocity start to deviate and eventually become very different [case (e)].

We find that for cases (a)–(c) both treatments—i.e., as an effective homogeneous medium with n_{eff} or as a periodic medium with the wave vector diagram formalism—give almost the same angle for the propagating beam. This value is in excellent agreement with the FDTD simulation result. Therefore, one might be tempted to describe a photonic crystal medium for cases with a low index contrast as a homogeneous medium with an index given by Eq. (22). However, the results we present in the following suggest that such a treatment would be erroneous. In fact, we consider the five different cases of Fig. 12. We take the same angle of incidence, but choose the interface along ΓM and, therefore, the propagation direction y along ΓK. We present our FDTD results in Fig. 13. Contrary to one's expectations for an effective homogeneous medium, even for a very low dielectric contrast [like 1.2:1 in case (b)], we observe three distinct refracted beams. These beams have propagating angles in excellent agreement with the predictions of a wave vector type of analysis in the repeated zone scheme as we described in Sec. III. Therefore we can infer that the wave "sees" the periodicity of the medium even when the index contrast is low. Conclusively, an effective medium approach fails for low-index-contrast cases lying in the higher bands. Note that even in an anisotropic homogeneous medium, at most, two refracted beams will be present, but never three as we observe in Fig. 13.

There is one interesting observation regarding the cases of Figs. 13(b) and 13(c). We checked, for each of the three refracted beams, the corresponding FB wave. We found that the FB wave describing each of these beams consists of only

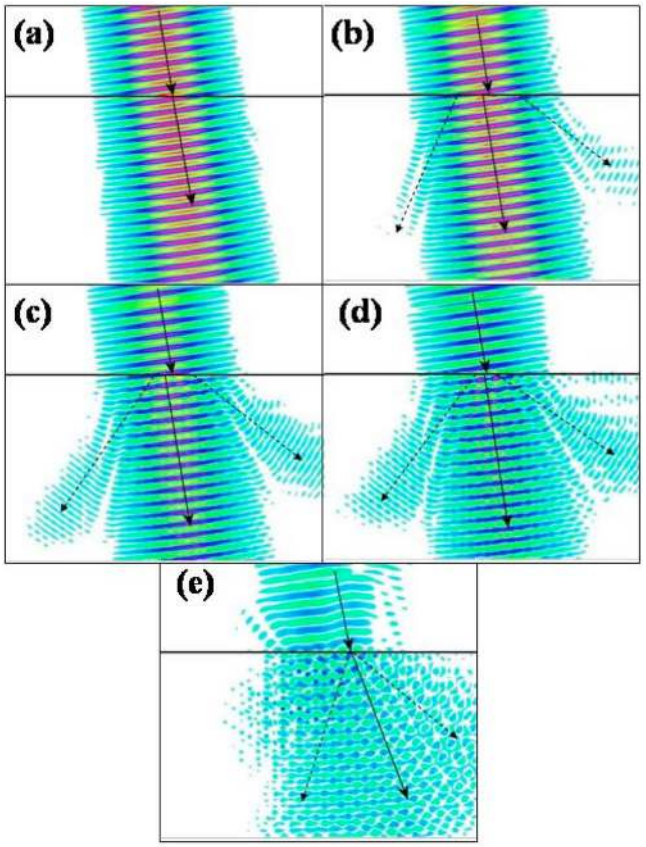

FIG. 13. (Color online) Refraction at oblique incidence with an angle of 8° for the same cases as in Fig. 13, but with ΓM as the symmetry direction of the interface. Even for a dielectric contrast as low as 1.2, one can see three distinct beams (although two of them are faint in magnitude).

one predominant coefficient. This lack of mixing in the FB sum for all beams in Figs. 13(b) and 13(c) manifests itself in the almost clear wave fronts, which brings us back to the discussion in Sec. IV regarding the appropriate definition for the phase velocity. In the cases of Figs. 13(b) and 13(c) for each beam, we have information as to how fast the phase given by $\mathbf{k}\cdot\mathbf{r}$ travels from point to point in space. So, in such cases, Yariv's picture [definition (5)] (Ref. 25) is appropriate. Therefore, it is natural to ask, when does Yariv's picture begin to fall apart? To answer this, we consider a similar numerical experiment as in Sec. V. We launch an EM wave normally onto the PC along the ΓM direction, which is the y direction. We sample the field at adjacent points in the numerical grid space, with respective coordinate y_i. Subsequently, we calculate the ratio $H(\omega,y_{i+1})/H(\omega,y_i)$. Here $H(\omega,y_i)$ represents the Fourier transform of the magnetic field $\mathbf{H}$, which is monitored in each time step at location y_i. The next step involves extracting a corresponding wave vector $\mathbf{k}$:

$$\mathbf{k} = \frac{1}{i\Delta y}\ln\left(\frac{H(\omega,y_{i+1})}{H(\omega,y_i)}\right)\hat{y}, \tag{26}$$

where $\Delta y = y_{i+1} - y_i = \sqrt{3}/62a$ is the size of the numerical grid along the propagation direction $\hat{y}$. Since Δy is small in this

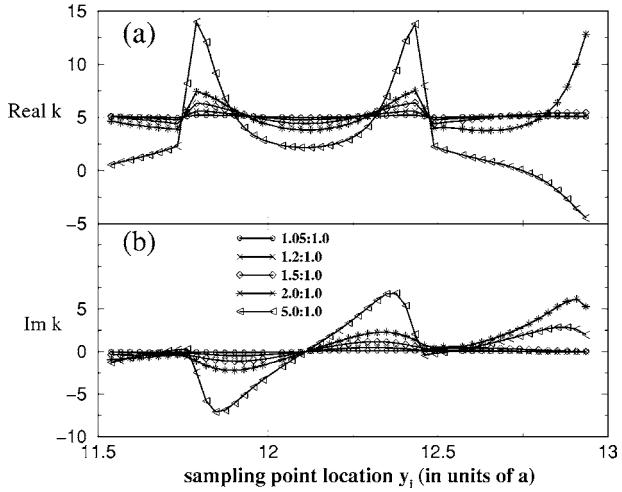

FIG. 14. (a) Real and (b) imaginary parts of the wave vector for the PC lattices of Figs. 12 and 13. The wave vector is calculated from the numerical FDTD field patterns at adjacent points y_i and $y_i+\Delta y$ [$\Delta y=(\sqrt{3}/62)a$]. We have taken normal incidence along ΓM and assumed in the wave vector extraction that one plane wave component dominates the propagation.

case, we take the principal value of the complex logarithm in Eq. (26). For a homogeneous system, such a process would lead to a wave vector which does not depend on the location y_i of the detector points. We plot the value of $\mathbf{k}$ given by Eq. (26) as a function of y_i. We show the corresponding real, k_R, and imaginary, k_I, parts for the five cases we analyze in this section in Figs. 14(a) and 14(b), respectively. Indeed, for case (a) this k_R is almost constant as it would be in a homogeneous medium. The small imaginary part present, is actually due to numerical errors. Nonetheless, as the index contrast increases, k_R ceases to be constant and starts showing increasingly higher variations with the location y_i. Moreover, an increasingly large imaginary part appears, contradictory to the fact that the photonic crystal is an inherently lossless system. Obviously, a phase velocity defined in the 2D crystal according to Yariv's picture[25] quickly breaks down as the index contrast increases. Thus, for the large-index-contrast cases, Notomi's picture[1] for the phase velocity (see Sec. IV) becomes appropriate.

The sign of "rightness" is equal to the sign of $\mathbf{S}\cdot\mathbf{k}$. Hence, it is closely related to the appropriate definition for the phase. We discussed in the previous sections that the "rightness" for the high-index-contrast PCs coincides with the slope of the relevant band. However, the band folding becomes an artificiality when the medium is homogeneous or when the index contrast is very low. Negative slope in such cases can by no means imply the existence of a left-handed (backwards) beam. The question arises, when is it appropriate to associate the sign of band slope with the sign of the "rightness"? All beams in Figs. 12(a)–12(c) and Figs. 13(a)–13(c) can very well be approximated by a plane wave. Therefore, clearly all the observed beams in such cases are right-handed beams. The cases of Figs. 12(d) and 13(d) have some small mixing, while the cases of Figs. 12(e) and 13(e) have a stronger mixing. As we also discussed before, only in cases with a strong mixing in the FB sum does the phase velocity associ-

ated with the wave vector in the first BZ have physical meaning. Consequently, only the latter cases qualify for possible left-handed behavior. In fact, we should attempt to discuss "rightness" only for cases where the real part k_R of the wave vector $\mathbf{k}$ calculated from Eq. (26) shows such large variations with the position y_i that it ranges from positive to negative values. This occurs only for case (e) where the dielectric contrast between the constituents is 5.0:1.0.

XI. COMPARISON WITH THE 1D LAYERED MEDIUM

The refractive properties of the 1D layered medium have been extensively studied.[10–14] However, there are significant differences between the properties of the 1D layered medium and the two-dimensional photonic crystal we studied in this paper. In the two-dimensional photonic crystal, when the plane of incidence is chosen to be the periodic plane, the entire wave vector is confined in the first BZ. In contrast, in the 1D periodic medium, only the component of the wave vector along the direction of periodicity is Bloch confined—i.e., restricted within the first BZ, in this case. This has several implications.

First, the modes in $\mathbf{k}$ space repeat themselves periodically in one direction only. If the interface is chosen along the 1D periodic direction, modes from the higher-order zones, in cases where $|\mathbf{k}_{\|}a/\pi|<1$, can never be accessed. One can access higher-order modes for small $|\mathbf{k}_{\|}|$ values only when a slanted interface is employed. This is the method used in Refs. 10 and 11 to access modes lying outside the first BZ with small $|\mathbf{k}_{\|}|$. However, in our 2D system we can access higher-order modes even when the interface is cut along a symmetry direction and small $|\mathbf{k}_{\|}|$. In fact, these are the refracted beams indicated with dotted line in the cases of Figs. 1(b) and 1(c) (higher-order beams of the first kind).

Second, the most important implication is regarding the "rightness." In the 2D system, a band with negative slope corresponds to a left-handed (backwards) beam. However, this is not true for a one-dimensional system. We have chosen x to represent the direction of the periodicity. The slope of a certain band will then be given by $\partial\omega(k_x,k_y)/\partial k_x$ or equivalently $v_{gx}k_x$, where v_{gx} is the component of the group velocity along the direction of periodicity. We use the $\mathbf{k}\cdot\mathbf{p}$ perturbation method to calculate v_{gx}.[53–55] We calculate the Poynting vector $\mathbf{S}$ with the use of the FB wave expansions for the 1D layered system. We obtain

$$\langle \mathbf{S}\rangle \cdot \mathbf{k} = \frac{c^2}{8\pi\omega}\left(k_y^2 A_\eta + \frac{\omega}{c^2} v_{gx} k_x\right), \tag{27}$$

where $\langle\cdots\rangle$ refers to the spatial average within the 1D unit cell of the time-averaged quantity and $\omega=\omega(k_x,k_y)$ for the band under consideration. In the case of H polarization (magnetic field is perpendicular to the plane of incidence),

$$A_\eta = \sum_{G,G'} \eta_{G,G'} H_G H_{G'} = \int \eta(x)|v|^2 dx, \tag{28}$$

with $\eta(x)=1/\epsilon(x)$ and $v=\sum_G H_G(k_x,k_y)e^{iGx}$ for the band under consideration. Since the integrand in expression (28) is positive, A_η is a positive definite quantity.[58]

Now, for a band with a positive slope, $v_{gx}k_x>0$ and so $\langle \mathbf{S}\rangle\cdot\mathbf{k}>0$. For a band with a negative slope $v_{gx}k_x<0$. Then $\langle \mathbf{S}\rangle\cdot\mathbf{k}<0$, only if

$$k_y^2 A_\eta < \frac{\omega}{c^2}|v_{gx}k_x|, \tag{29}$$

where k_x is within the limits of the 1D BZ.

In other words, a propagating wave that corresponds to a band with positive slope is always a forward wave. In contrast, a propagating wave that corresponds to a band with a negative slope is backwards (left-handed) only when condition (29) is satisfied. Note that condition (29) holds, regardless of the choice of the interface, provided that x represents the stacking (periodic) direction and y the direction perpendicular to this. If we choose the interface along y and consider normal incidence, then $k_y=0$. Thus, in this particular case, a band with negative slope yields a backwards wave. Furthermore, we examined this condition for a case with high-index modulation, H polarization, frequency falling in the second band, and interface along the x direction. We employed the PWE method[42–44] and found that the possibility of left-handed behavior is restricted only to a small fraction of frequencies of the second band. In addition, for the applicable frequencies, one obtains backwards waves only for a part of the wave vector space. So, for the 1D layered medium, a negative slope does not necessarily imply a backwards beam. Each individual case should be examined with condition (29) to determine the "rightness" of the propagating beam. We note at this point that the backwards coupling[59] observed between two waveguides linked with 1D layered medium does not necessarily imply a backwards wave.

XII. CONCLUSIONS

We systematically studied EM wave propagation in two-dimensional photonic crystal structures. We based our analysis on the wave vector diagram formalism. We observed different cases where negative refracted beam with distinctly different origins are present. We confirmed that the condition for single-beam propagation does not coincide with the condition for having a single reflected beam in the incoming medium. For simple cases, we determined the conditions for single-beam propagation and applicability of Snell's formula. We revisited the controversial topic of phase velocity and showed that in a photonic crystal with strong scattering present, only the wave vector inside the first BZ zone has physical meaning. We used the symmetry properties of the photonic crystal to appropriately design a wedge experiment that can determine the "rightness" of a general 2D PC system (triangular or square). We studied the behavior of the PC system as the index contrast transitions from high to low values. With the rapid development of photonic crystals more complicated structures are now fabricated—for example, 12-fold symmetrical quasicrystals.[60] In more complicated structures,[36,60] the wave vector diagram analysis should be performed in its general form, as presented in Sec. III. We believe our systematic study will aid the understanding of

EM propagation in three-dimensional structures. In 3D structures, interesting phenomena may arise because of the possibility of polarization coupling. Moreover, the present study will help in the designing of appropriate PC-based superlenses, which have been attracting increasing interest, both theoretical[3,61,62] and experimental.[63] Our work is also relevant to optical devices such as light deflection devices,[64] waveguide division multiplexers,[65] etc.

ACKNOWLEDGMENTS

We thank P. St. Russell and E. N. Economou for useful discussions. We also thank Kurt Busch for his help with the $\mathbf{k}\cdot\mathbf{p}$ perturbation method and useful discussion. Ames Laboratory is operated by the U.S Department of Energy by Iowa State University under Contract No. W-7405-Eng-82. This work was partially supported by DARPA (Contract No. MDA972-01-2-0016) and by the EU FET project DALHM.

APPENDIX

1. Higher-order Bragg reflected beams

For the cases indicated in Eq. (R1), the $k_{\parallel,m}$ component of an order m Bragg reflected wave in the air medium is given by Eq. (1). In order not to have any Bragg waves for any angle of incidence the condition

$$\left|\frac{\omega}{c}\sin\theta_{inc}+\frac{2m\pi}{b_{per}}\right|>\omega/c \tag{A1}$$

must be observed, $\forall m\neq 0$, $\forall|\theta_{\mathrm{inc}}|\epsilon[0,\pi/2]$.

But if

$$\frac{\omega}{c}\sin\theta_{inc}>\frac{2\pi}{b_{per}}, \tag{A2}$$

then

$$\left|\frac{\omega}{c}\sin\theta_{inc}-\frac{2\pi}{b_{per}}\right|=\frac{\omega}{c}\sin\theta_{inc}-\frac{2\pi}{b_{per}}<\frac{\omega}{c}\sin\theta_{inc}<\frac{\omega}{c}, \tag{A3}$$

i.e., a Bragg wave of order $m=-1$ couples. Therefore, the first condition we must impose is

$$\frac{\omega}{c}\sin\theta_{inc}<\frac{2\pi}{b_{per}}, \tag{A4}$$

$\forall|\theta_{inc}|<\pi/2$. Equivalently,

$$\frac{\omega}{c}<\frac{2\pi}{b_{per}} \tag{A5}$$

must be satisfied. Assuming this condition is valid, we proceed:

$$\left|\frac{\omega}{c}\sin\theta_{inc}+\frac{2m\pi}{b_{per}}\right|\geqslant\min\left(\left|\frac{\omega}{c}\sin\theta_{inc}+\frac{2m\pi}{b_{per}}\right|\right)\geqslant\left|\frac{\omega}{c}-\frac{2\pi}{b_{per}}\right|. \tag{A6}$$

So it suffices to find the frequencies to satisfy

$$\left|\frac{\omega}{c}-\frac{2\pi}{b_{per}}\right|>\frac{\omega}{c} \tag{A7}$$

or, equivalently,

$$\tilde{f}\leqslant\frac{a}{2b_{per}}, \tag{A8}$$

with a being the lattice constant and b_{per} given by Eq. (R1).

No higher-order reflected beams appear for any angle of incidence for frequencies satisfying Eq. (A8). If condition (A8) [or (A7)] is valid, condition (A5) is automatically satisfied. In addition, for a certain frequency satisfying (A5), for a certain incident angle θ_{inc} obeying the inequality,

$$-\frac{\omega}{c}\sin\theta_{inc}+2\pi/b_{per}>\frac{\omega}{c}, \tag{A9}$$

no higher-order Bragg reflected beams appear.

2. Equivalent points in wave vector space

The eigenvalue equation that results from expression (4) and Maxwell's equation is for the H-polarization case,[56]

$$\sum_{\mathbf{G}'}\eta_{\mathbf{G},\mathbf{G}'}(\mathbf{k}+\mathbf{G})\cdot(\mathbf{k}+\mathbf{G}')H_{\mathbf{G}'}(\mathbf{k})=\frac{\omega^2}{c^2}H_{\mathbf{G}}(\mathbf{k}). \tag{A10}$$

Suppose we consider the FB wave for $\mathbf{K}=\mathbf{k}+\mathbf{G}_0$ with $\mathbf{G}_0$ a reciprocal lattice vector. Then, the eigenvalue equation becomes

$$\sum_{\mathbf{G}'}\eta_{\mathbf{G},\mathbf{G}'}(\mathbf{k}+\mathbf{G}+\mathbf{G}_0)\cdot(\mathbf{k}+\mathbf{G}'+\mathbf{G}_0)H_{\mathbf{G}'}(\mathbf{K})=\frac{\omega^2}{c^2}H_{\mathbf{G}}(\mathbf{K}). \tag{A11}$$

From Eq. (A11) after setting $\mathbf{G}_1=\mathbf{G}+\mathbf{G}_0$ and $\mathbf{G}_2=\mathbf{G}'+\mathbf{G}_0$ we get

$$\sum_{\mathbf{G}_2}\eta_{\mathbf{G}_1,\mathbf{G}_2}(\mathbf{k}+\mathbf{G}_1)\cdot(\mathbf{k}+\mathbf{G}_2)H_{\mathbf{G}_2-\mathbf{G}_0}(\mathbf{K})=\frac{\omega^2}{c^2}H_{\mathbf{G}_1-\mathbf{G}_0}(\mathbf{K}). \tag{A12}$$

By comparison with the original eigenvalue equation, it is evident that

$$H_{\mathbf{G}-\mathbf{G}_0}(\mathbf{K})=H_{\mathbf{G}}(\mathbf{k}). \tag{A13}$$

Therefore, the time-independent part of the FB wave [Eq. (4)] for $\mathbf{K}$ becomes

$$\begin{aligned}H_{FB,\mathbf{K}}&=e^{i\mathbf{K}\cdot\mathbf{r}}\sum_{\mathbf{G}}H_{\mathbf{G}}(\mathbf{K})e^{i\mathbf{G}\cdot\mathbf{r}}=e^{i\mathbf{k}\cdot\mathbf{r}}\sum_{\mathbf{G}}H_{\mathbf{G}}(\mathbf{K})e^{i(\mathbf{G}+\mathbf{G}_0)\cdot\mathbf{r}}\\&=e^{i\mathbf{k}\cdot\mathbf{r}}\sum_{\mathbf{G}'}H_{\mathbf{G}'-\mathbf{G}_0}(\mathbf{K})e^{i\mathbf{G}'\cdot\mathbf{r}}=e^{i\mathbf{k}\cdot\mathbf{r}}\sum_{\mathbf{G}'}H_{\mathbf{G}'}(\mathbf{k})e^{i\mathbf{G}'\cdot\mathbf{r}}\\&=H_{FB,\mathbf{k}}.\end{aligned} \tag{A14}$$

So the Floquet-Bloch wave expressions corresponding to wave vectors $\mathbf{k}$ and $\mathbf{K}$, separated by a reciprocal lattice vec-

tor $\mathbf{G}_0$, are equivalent. In other words, $\mathbf{k}$ and $\mathbf{K}$ are equivalent points in wave vector space.

3. Yariv's definition for the phase velocity

In the 1D system the wave vector in the plane of incidence is not confined in the first BZ, but only the component along the periodicity. Therefore, the FB wave has the form (when magnetic field perpendicular to the plane of incidence)

$$\mathbf{H}(\mathbf{r},t) = e^{ikx}e^{i\beta y}\sum_G H_G(k,\omega)e^{iGx}e^{-i\omega t}\hat{z}. \tag{A15}$$

x is chosen to represent the direction of periodicity. The phase velocity defined in Ref. 25 for the FB wave, given by Eq. (A15) is

$$v_p = \frac{c}{\sqrt{k^2+\beta^2}}. \tag{A16}$$

In this expression (see Ref. 25), k is not within the first BZ zone, but chosen so that $|H_0| > |H_G| \forall G \neq 0$.

4. Average of the FB wave in the Wigner-Seitz cell

From Eq. (4) we get,

$$\begin{aligned}\langle H(\mathbf{r}=\mathbf{R})\rangle &= \frac{1}{\sqrt{A_{WS}}}e^{-i\omega t}\int_{\mathbf{r}'} e^{i\mathbf{k}\cdot(\mathbf{R}+\mathbf{r}')}\sum_{\mathbf{G}} H_{\mathbf{G}}e^{i\mathbf{G}\cdot(\mathbf{R}+\mathbf{r}')}d^2\mathbf{r}' \\ &= \frac{1}{\sqrt{A_{WS}}}e^{-i\omega t}e^{i\mathbf{k}\cdot\mathbf{R}}\int_{\mathbf{r}'} e^{i\mathbf{k}\cdot\mathbf{r}'}\sum_{\mathbf{G}} H_{\mathbf{G}}e^{i\mathbf{G}\cdot\mathbf{r}'}d^2\mathbf{r}' \\ &= e^{-i\omega t}e^{i\mathbf{k}\cdot\mathbf{R}}\langle H(\mathbf{r}=0)\rangle,\end{aligned} \tag{A17}$$

where $\mathbf{r}'$ ranges within the Wigner-Seitz cell around $\mathbf{r}=\mathbf{R}$, $\mathbf{R}$ is a Bravais lattice vector, and we used $e^{i\mathbf{G}\cdot\mathbf{R}}=1$.

*Current address: Laboratoire de Physique du Solide, Facultés Universitaires Notre-Damme de La Paix, B-5000 Namur, Belgium. Electronic address: sfoteino@fundp.ac.be

[1] M. Notomi, Phys. Rev. B **62**, 10696 (2000).
[2] B. Gralak, S. Enoch, and G. Tayeb, J. Opt. Soc. Am. A **17**, 1012 (2000).
[3] C. Luo, S. G. Johnson, J. D. Joannopoulos, and J. B. Pendry, Phys. Rev. B **65**, 201104(R) (2002).
[4] C. Luo, S. G. Johnson, J. D. Joannopoulos, and J. B. Pendry, Phys. Rev. B **68**, 045115 (2003).
[5] S. Foteinopoulou and C. M. Soukoulis, Phys. Rev. B **67**, 235107 (2003).
[6] H. Kosaka, T. Kawashima, A. Tomita, M. Notomi, T. Tamamura, T. Sato, and S. Kawakami, Phys. Rev. B **58**, R10096 (1998).
[7] E. Cubukcu, K. Aydin, E. Ozbay, S. Foteinopoulou, and C. M. Soukoulis, Nature (London) **423**, 604 (2003).
[8] M. Born and E. Wolf, *Principles of Optics: Electromagnetic Theory of Propagation, Interference and Diffraction of Light* (Pergamon Press, New York, 1980).
[9] J. P. Mathieu, *Optics* (Pergamon Press, New York, 1975).
[10] P. St. J. Russell, Appl. Phys. B: Photophys. Laser Chem. **39**, 231 (1986).
[11] P. St. J. Russell, T. A. Birks, and F. Dominic Lloyd-Lucas, in *Confined Electrons and Photons, New Physics and Applications*, Vol. 340 of *NATO Advanced Studies Institute, Series B: Physics*, edited by E. Burstein and C. Weisbuch (Plenum, New York, 1995), p. 585.
[12] P. St. Russell and T. A. Birks in *Photonic Band Gap Materials*, Vol. 315 of *NATO Advanced Studies Institute, Series E: Applied Sciences*, edited by C. M. Soukoulis (Kluwer, Dordrecht, 1996), p. 71.
[13] P. St. J. Russell, Phys. Rev. A **33**, 3232 (1986).
[14] R. Zengerle, J. Mod. Opt. **34**, 1589 (1987).
[15] H. Kosaka, T. Kawashima, A. Tomita, M. Notomi, T. Tamamura, T. Sato, and S. Kawakami, J. Lightwave Technol. **17**, 2032 (1999).
[16] V. G. Veselago, Usp. Fiz. Nauk **92**, 517 (1964) [Sov. Phys. Usp. **10**, 509 (1968)].
[17] D. R. Smith, W. J. Padilla, D. C. Vier, S. C. Nemat-Nasser, and S. Schultz, Phys. Rev. Lett. **84**, 4184 (2000); R. A. Shelby, D. R. Smith, S. C. Nemat-Nasser, and S. Schultz, Appl. Phys. Lett. **78**, 489 (2001).
[18] J. B. Pendry, A. J. Holden, W. J. Stewart, and I. Youngs, Phys. Rev. Lett. **76**, 4773 (1996); J. B. Pendry, A. J. Holden, D. J. Robbins, and W. J. Stewart, J. Phys.: Condens. Matter **10**, 4785 (1998); IEEE Trans. Microwave Theory Tech. **47**, 2075 (1999); J. B. Pendry, Phys. Rev. Lett. **85**, 3966 (2000).
[19] D. R. Smith, S. Schultz, P. Markoš, and C. M. Soukoulis, Phys. Rev. B **65**, 195104 (2002).
[20] P. A. Belov, Microwave Opt. Technol. Lett. **37**, 259 (2003).
[21] The PC structure is periodic in space. Therefore whenever we refer to **S** in the PC, the spatial average within the unit cell of the time-averaged Poynting vector is considered.
[22] A. Taflove, *Computational Electrodynamics—The Finite Difference Time-Domain Method* (Artech House, Boston, 1995).
[23] R. A. Shelby, D. R. Smith, and S. Schultz, Science **77**, 292 (2001).
[24] C. G. Parazzoli, R. B. Greegor, K. Li, B. E. C. Koltenbah, and M. Tanielian, Phys. Rev. Lett. **90**, 107401 (2003).
[25] A. Yariv and P. Yeh, *Optical Waves in Crystals: Propagation and Control of Laser Radiation* (Wiley, New York, 1984).
[26] H. Kosaka, A. Tomita, T. Kawashima, T. Sato, and S. Kawakami, Phys. Rev. B **62**, 1477 (2000).
[27] S. Datta, C. T. Chan, K. M. Ho, and C. M. Soukoulis, Phys. Rev. B **48**, 14936 (1993).
[28] K. S. Yee, IEEE Trans. Antennas Propag. **14**, 302 (1966).
[29] J.-P. Berenger, J. Comput. Phys. **114**, 185 (1994); J.-P. Berenger, IEEE Trans. Antennas Propag. **44**, 110 (1996).
[30] J. D. Jackson, *Classical Electrodynamics* (Wiley, New York, 1999).
[31] This concerns cases with interface chosen along the stacking direction, which is the only symmetry direction for the 1D gratings system.
[32] S. Ponti and C. Oldano, Phys. Rev. E **67**, 036616 (2003).

[33] K. Sakoda, *Optical Properties of Photonic Crystals* (Springer, Berlin, 2001).

[34] It can be checked that if *all* infinite number of reciprocal lattice vectors are projected onto an "arbitrary" slanted interface, the spacings between the corresponding adjacent projections are zero. This implies an infinite number of reflected beams and an infinite number of refracted beams. However, in practice only a *finite*, number of reciprocal lattice vectors make a non-negligible contribution to the Floquet-Bloch wave [expression (4)]. This is true even for cases with a high-index modulation. In other words, in realistic examples a finite set of reciprocal lattice vectors suffices in the repeated zone scheme of the wave vector diagram or equivalently in determining the applicable phase matching condition. As a consequence, in realistic examples one observes only a finite number of distinct dominant beams (reflected and refracted). We studied a particular case of a triangular PC with a slanted interface at 20° with the ΓM symmetry directions. Our results show an excellent agreement between the wave vector diagram predictions and FDTD. We remark that by an "arbitrary" slanted interface we mean an interface at an angle θ with a certain symmetry direction, with $\tan\theta/\sqrt{3}$ ($\tan\theta$) being an irrational number for the case of triangular (square) lattices.

[35] A. I. Cabuz, E. Centeno, and D. Cassagne, Appl. Phys. Lett. **84**, 2031 (2004).

[36] X. Wang, Z. F. Ren, and K. Kempa, Appl. Phys. Lett. **86**, 061105 (2005).

[37] The diamond lattice is a face-centered-cubic (FCC) lattice with a basis. However, when cut along the [1, 1, 0] plane it will be subject to a different phase matching condition from the underlying FCC lattice. This is because for the case of a diamond lattice, only the projections of those reciprocal lattice vectors with a non-vanishing structure factor [38], contribute towards the phase matching. Moreover, examples of 2D PCs with a basis show that the phase matching condition for a particular interface may not follow the Bragg formula of the corresponding 1D lattice.

[38] N. W. Ashcroft and N. D. Mermin, Solid State Physics (Saunders College Publishing, 1976)

[39] While this paper was under review S. Yu and S. Fan [Phys. Rev. E **70**, 055601(R) (2004)] reported anomalous reflections for beams incident from inside a PC on an arbitrary slanted interface. They also use a generalized phase matching condition, based on the projections of all reciprocal lattice vectors onto the interface.

[40] L. Brillouin, *Wave Propagation in Periodic Structures* (Dover, New York, 1953).

[41] Usually, in the 1D literature the predominant wave vector of the FB sum is called a fundamental wave vector. In order to keep our analysis general, even for cases with very strong mixing in the FB sum, we choose the wave vector in the first zone to call as fundamental wave vector. See also the Appendix, Part 2.

[42] K. M. Ho, C. T. Chan, and C. M. Soukoulis, Phys. Rev. Lett. **65**, 3152 (1990).

[43] P. R. Villeneuve and M. Piche, Prog. Quantum Electron. **18**, 153 (1994).

[44] K. M. Ho, C. T. Chan, and C. M. Soukoulis, in *Photonic Band Gaps and Localization*, Vol. 308 of *NATO Advanced Studies Institute, Series B: Physics*, edited by C. M. Soukoulis (Plenum, New York, 1992), p. 235.

[45] L. Li, J. Opt. Soc. Am. A **13**, 1870–1876 (1996).

[46] S. Foteinopoulou, E. N. Economou, and C. M. Soukoulis, Phys. Rev. Lett. **90**, 107402 (2003).

[47] A. Yariv and P. Yeh, J. Opt. Soc. Am. A **67**, 438 (1977).

[48] A. Kirchner, K. Busch, and C. M. Soukoulis, Phys. Rev. B **57**, 277 (1998).

[49] R. W. Ziolkowski and E. Heyman, Phys. Rev. E **64**, 056625 (2001).

[50] W. H. Press, B. P. Flannery, S. A. Teukolsky, and W. T. Vetterling, *Numerical Recipes: The art of scientific computing* (Cambridge University Press, Cambridge, England, 1986).

[51] The discrepancy is mainly due to the dicsretization in the FDTD simulation. In fact, if in the EFS analysis we use the discretized dielectric function instead, we obtain a wave vector value of $k=-2.26a^{-1}$.

[52] P. Yeh, J. Opt. Soc. Am. A **69**, 742–756 (1979).

[53] N. F. Johnson, P. M. Hui, and K. H. Luk, Solid State Commun. **90**, 229 (1994).

[54] K. Busch, M. Frank, A. Garcia-Martin, D. Hermann, S. F. Mingaleev, M. Schillinger, and L. Tkeshelashvili, Phys. Status Solidi A **197**, 637 (2003); (private communication).

[55] D. Hermann, M. Frank, K. Busch, and P. Wölfle, Opt. Express **8**, 167 (2001).

[56] $\eta_{\mathbf{G}_1,\mathbf{G}_2}$ are the matrix elements corresponding to the inverse of matrix $[\epsilon]_{\mathbf{G}_1,\mathbf{G}_2}$, which represents the Fourier transform of the dielectric function.

[57] J. A. Buck, *Fundamentals of Optical Fibers* (Wiley-Interscience, New York, 1995).

[58] If the fields were E-polarized, the quantity A_η in Eq. (45) would be $\Sigma E_{\mathbf{G}}^2$. Thus, in this case too, it will be positive definite.

[59] P. Yeh and H. F. Taylor, Appl. Opt. **19**, 2848 (1980).

[60] M. E. Zoorob, M. D. B. Charlton, G. J. Parker, J. J. Baumberg, and M. C. Netti, Nature (London) **404**, 740 (2000).

[61] R. Moussa, S. Foteinopoulou, Lei Zhang, G. Tuttle, K. Guven, E. Ozbay, and C. M. Soukoulis, Phys. Rev. B **71**, 085106 (2005).

[62] X. Wang, Z. F. Ren, and K. Kempa, Opt. Express **12**, 2919 (2004).

[63] E. Cubukcu, K. Aydin, E. Ozbay, S. Foteinopoulou, and C. M. Soukoulis, Phys. Rev. Lett. **91**, 207401 (2003).

[64] T. Baba and M. Nakamura, IEEE J. Quantum Electron. **38**, 909 (2002).

[65] L. J. Wu, M. Mazilu, T. Karle, and T. F. Krauss, IEEE J. Quantum Electron. **38**, 915 (2002).